M. Sc. Global Change Geography

Master Thesis

Analysis of micro-climate variation and feedbacks in an Arctic tundra landscape on Disko Island, Western Greenland

Laura Becker

Supervisors:

Dr. Simone M. Stünzi,
Prof. Dr. Julia Boike

Submitted to the Department of Geography,
Humboldt-Universität zu Berlin

Berlin, December 10, 2024

Abstract

The Arctic tundra is experiencing rapid changes due to climate warming, with profound implications for permafrost ecosystems and their feedbacks to the global climate. Vegetation changes driven by precipitation and temperature increases include extended shrub cover and increases in plant primary production. Changes in vegetation and climate alter soil moisture and temperature on small spatial scales (< 1 m), which mediate greenhouse gas sequestration and emission processes during summer. Understanding these interactions is essential for identifying climate feedback mechanisms and supporting global assessments using remote sensing data.

This study examines the relationships between vegetation cover, topography, surface soil moisture and their effects on soil temperature in an Arctic tundra landscape on Disko Island (*Qeqertarsuaq*), Western Greenland. Data were collected from 24 sites (1 m²) in a southern valley on Disko Island during field studies conducted between September 2022 and September 2024. It includes visually assessed vegetation cover, a digital terrain model and continuous temperature-moisture data collected using TOMST TMS-4 sensors. I derived variables describing vegetation (vegetation height, vegetation density, forb, graminoid, lichen, moss and shrub cover) and topography (elevation, geomorphon type and slope). I quantified the spatial and annual variation of summer mean soil temperature and moisture at the study site during the summer seasons of 2023 and 2024. I then used single linear regression models to identify the variables which explained most of the variance in the moisture and temperature data of the summer season 2023.

Mean summer surface soil moisture varied between 14% and 60%, mean summer soil temperatures between 1.9 °C and 6.5 °C. The linear regression models revealed that geomorphon type (R = 0.35), graminoid cover (R^2 = 0.35) and slope (R^2 = 0.28) were most important predictors of summer soil surface moisture, with higher soil moisture in sheltered and flatter locations with high graminoid cover. Summer soil temperature was best explained by slope (R^2 = 0.25), elevation (R^2 = 0.23), graminoid cover (R^2 = 0.15) and lichen (R^2 = 0.12), exhibiting cooler soils at higher elevations with steeper terrain and less graminoid cover whereas high lichen cover indicated warmer soils in summer. Contrary to prior expectations, shrub and moss cover explained little variance in both soil moisture and temperature (< 10% and < 5%, respectively).

These findings underscore the dominant role of topography in shaping summer soil microclimate, while also highlighting the influence of vegetation, particularly graminoid cover. Future vegetation changes in Arctic landscapes are likely to alter soil thermal and hydrological regimes, with implications for greenhouse gas fluxes. Investigating interactions between vegetation, soil moisture, and temperature across diverse topographic settings is essential for predicting feedbacks to climate change.

CONTENTS

LIST OF TABLES

LIST OF FIGURES

1 INTRODUCTION

The mean annual air temperature in the Arctic increased by 3.1 °C between 1971 and 2019, three times as much as the global average. That is accompanied by a decrease in snow cover extent and increasing liquid precipitation, resulting in rising permafrost temperatures (Biskaborn et al., 2019; AMAP, 2021). Approximately 15% of the exposed land surface in the Northern Hemisphere display permafrost, which is defined as ground that remains below 0 °C for at least two consecutive years (Obu, 2021). Northern circumpolar permafrost is estimated to store up to 50% of the global below ground organic carbon (Tarnocai et al., 2009). Rising permafrost temperatures trigger the release of the greenhouse gases carbon dioxide and methane because of increased microbial activity in the thawing soil. This in turn creates a positive feedback on climate change (Olefeldt et al., 2013; Schuur et al., 2015).

In response to the rapidly rising temperatures, a prolonged growing season and increased water availability due to permafrost thaw and changes in precipitation patterns, Arctic tundra ecosystems are experiencing several notable shifts. These include increases in plant productivity and height (Elmendorf et al., 2012; Guay et al., 2014; Bjorkman et al., 2018) as well as a shift in species composition (Elmendorf et al., 2015) and tall shrub expansion (García Criado et al., 2020; Heijmans et al., 2022) over extended temporal scales. The resulting vegetation change in return has the potential to increase annual net soil temperatures (Heijmans et al., 2022) and alter soil temperature on short temporal scales, thereby creating another positive feedback loop by promoting further shrub encroachment (Sturm et al., 2005; Chapin III et al., 2005).

Soil temperatures in the Arctic result from a complex interplay of abiotic and biotic factors that alter the energy partitioning of the incoming solar radiation (Oehri et al., 2022). This includes meteorological conditions (e.g. air temperature, cloudiness), ground surface properties (e.g. albedo, roughness), ground thermal properties (e.g. heat conductivity), topography, soil moisture, snow cover and vegetation (Fig. 1). These factors influence the net amount of incoming radiation and the magnitude of the sensible, latent and ground heat flux, which together are responsible for warming and cooling of the ground and near-ground air. (Loranty et al., 2018)

The contribution of different heat fluxes to soil temperatures varies both seasonally and spatially across the diverse Arctic landscape (Oehri et al., 2022). In winter, snow is the

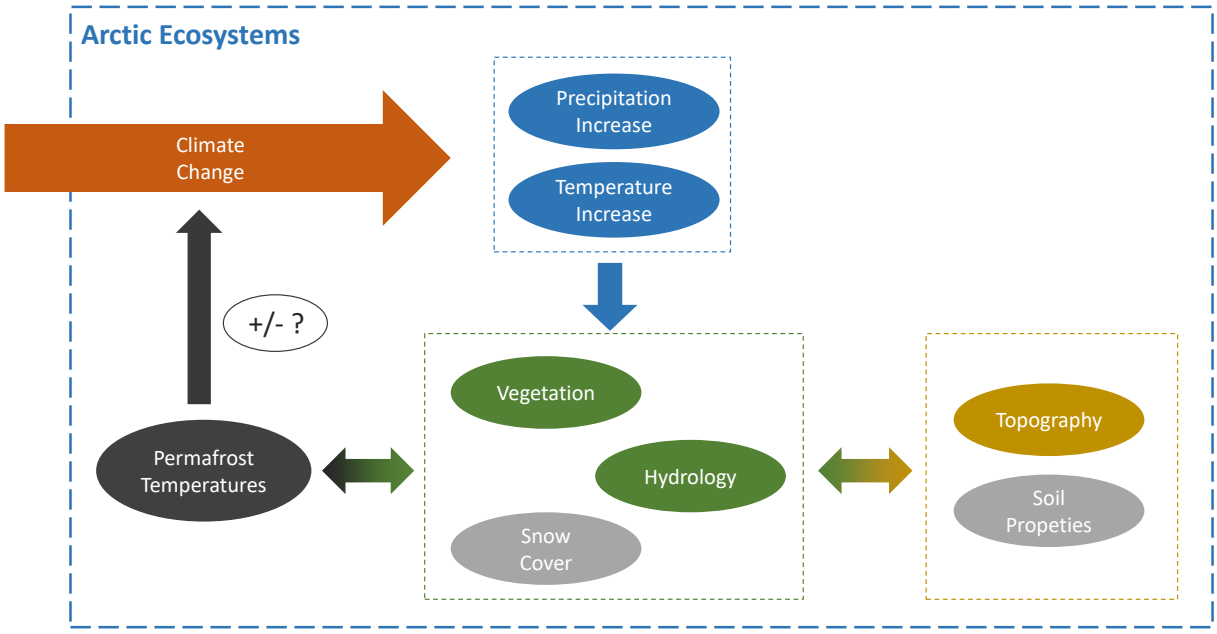

Figure 1: Schematic representation of climate change impacts on Arctic ecosystems. Rising air temperatures and liquid precipitation drive changes in vegetation, hydrology, and snow cover, which in turn influence permafrost temperatures. Vegetation, hydrology and snow cover are mediated by landscape characteristics, including soil conditions and topography. Shifts in permafrost temperatures can in turn change vegetation composition, hydrology, snow cover and alter greenhouse gas emissions, creating feedback loops that either amplify or mitigate climate change, depending on the interactions among the individual components. Observations of snow cover and soil properties are not included in this study.

main surface cover and there is only little to no incoming solar radiation. Hence, winter soil temperatures are mostly mediated by snow cover: High albedo and low heat conductivity contribute to the insulating effect of snow, leading to warmer soils under deeper snow cover (Zhang, 2005; Grünberg et al., 2020). Initially, snowfall determines snow accumulation patterns, but by re-distribution through wind, vegetation and topography gain importance in the distribution of snow. Snow-trapping characteristics of shrub canopies can increase winter soil temperatures at shrub sites (Sturm et al., 2001; Myers-Smith and Hik, 2013; Frost et al., 2018; Von Oppen et al., 2022), while snowdrift off of wind-blown ridges can lead to cooler soils at exposed topographic positions (Sundstøl and Odland, 2017).

In summer, surface cover is more diverse and the amount of incoming radiation increases. The share of radiation reaching the surface depends on topographical position, which leads to cooler soils on north exposed slopes (Aartsma et al., 2023), in depressions or shady locations (Aalto et al., 2018). Vegetation interception further reduces the amount of radiation directly reaching the ground. Typical tundra vegetation grows in patches and consists of low-growing plant types such as mosses, lichen, sedges, grasses, rushes

and shrubs (Walker et al., 2005). The comparably low albedo of dark shrub canopies increases energy absorption at shrub sites and leads to a warming of the surrounding air (Eugster et al., 2000; Chapin III et al., 2005). Despite rising air temperatures, shrub cover reduces summer soil temperatures and dampens daily temperature amplitudes due to shading effects and increased evapotranspiration (Blok et al., 2010; Myers-Smith and Hik, 2013; Aartsma et al., 2023). The increased evapotranspiration and rainfall interception at shrub sites can cause drier ground conditions, lowering the heat conductivity of the soil and thereby improving the insulation of the soil from air (O'Donnell et al., 2009). Litter layers under shrub canopies additionally insulate soils from warm air temperatures and offset daily thermal dynamics (Heijmans et al., 2022; Aartsma et al., 2023). Soil cooling effects have also been observed under lichen cover, due to the high surface albedo (Aartsma et al., 2023; Mallen-Cooper et al., 2021). Mosses (non-vascular plants) and organic layers (often found in the topsoil of tundra landscapes) have varying effects on soil temperature, depending on their thickness and moisture content (Schuuring et al., 2024; Gonzalez Martinez et al., 2023). While cooling effects under insulating layers of moss have been observed (Blok et al., 2011; Gornall et al., 2007), increasing moisture content of the moss layer increases heat conductivity and reduces the insulation of underlying soil (Soudzilovskaia et al., 2013; Loranty et al., 2018).

Besides local climate, topography and vegetation cover, soil moisture plays a critical role in shaping summer soil temperatures by influencing the thermal and surface properties of the ground and surface cover, including heat capacity, thermal conductivity, and albedo (Legates et al., 2011). Understanding the implications of changes in air temperature, precipitation, and vegetation on soil moisture is particularly important because soil moisture mediates greenhouse gas emission processes in the Arctic (Lawrence et al., 2015; Natali et al., 2015), thereby amplifying or mitigating climate change feedbacks. These feedback mechanisms can operate directly, by affecting ground-level decomposition or carbon sequestration processes, or indirectly, for example, by limiting plant productivity during summer due to reduced moisture availability (Zona et al., 2023). Additionally, moisture scarcity can prevent the formation of highly insulative snow layers over dry soils, leading to colder soil conditions during winter (Domine et al., 2018). Observations of warmer soil temperatures and deeper active layer thaw depths in wet soils further suggest that the increased heat conductivity in such conditions may outweigh the effects of higher heat capacity and

evaporation in deeper soil layers (Shiklomanov et al., 2010). However, studying soil moisture and its interactions with soil temperature remains challenging due to the regulation of soil moisture by numerous interdependent factors. Topography, for example, directly influences soil moisture by concentrating water in depressions while reducing it on slopes (Scherrer and Körner, 2011), and indirectly by shaping snow accumulation patterns. Intrinsic soil properties, such as porosity and texture, determine the soil's water-holding capacity (Legates et al., 2011). Vegetation also plays a key role in mediating soil moisture levels, for instance, by intercepting rainfall and controlling evaporative losses (Aalto et al., 2013; Zwieback et al., 2019). Finally, snow accumulation is a significant predictor of summer soil moisture, particularly when summer rainfall is limited (Litaor et al., 2008).

Variations in topography, vegetation, and soil properties create a heterogeneous Arctic tundra landscape, leading to diverse soil moisture and temperature patterns. Their interactions result in highly localized soil temperature and moisture regimes, varying at small spatial scales ($\leq$ 1 m) (Aalto et al., 2013) and differing significantly from local air temperature measurements (Von Oppen et al., 2022). But contrary to the assumption that ecological relationships vary with the scale of observation (Wiens, 1989), Von Oppen et al. (2022) found that fine-scale temperatures (microclimate, $\leq$ 1m) extrapolated from local macroclimate using vegetation type as a predictor remained consistent across vegetation sampling plots of varying sizes (1–11.3 m in diameter). These findings suggest that understanding processes at fine spatial scales can help account for small-scale soil temperature variability in models based on coarse-resolution data, such as remote sensing imagery. Upscaling studies like Von Oppen et al. (2022) demonstrate that fine-scale ground observations can be effectively linked to remote sensing data, bridging gaps in permafrost temperature monitoring and improving estimates of climate change feedbacks on global scales.

This study investigates the relationships between soil temperature (at 6 cm depth), soil surface moisture (upper 0-15 cm, further called soil moisture), vegetation cover and topographic variables at the sub-meter scale during the 2023 summer season in a study area in the South of Disko Island, Western Greenland. While the driving factors of soil temperature in winter have been studied extensively, less research has been conducted on summer soil temperatures (Heijmans et al., 2022). Studying the interactions between vegetation and topography and their effects on soil temperature is crucial, because the balance of summer cooling and winter warming of soils varies significantly across diverse permafrost environ-

ments, ultimately determining the long term integrity of the permafrost soils. While recent research has focused on the impact of shrub cover on soil temperatures (Heijmans et al., 2022; Zhang, 2005), other Arctic tundra vegetation types remain relatively understudied.

My research question (**Q**), objectives (**O**) and hypotheses (**H**) are the following:

Q1 What are the links between vegetation, topography and soil moisture during summer and to which extent can they explain the temperature variations at the study site?

- **O1** Quantify the soil temperature variations at the study site.
  - **H1** Significant deviations of mean summer soil temperatures from local air temperature.
- **O2** Quantify the relationship between soil moisture, vegetation and topography.
  - **H1** Vegetation influences soil moisture and vice versa, e.g. shrub sites exhibit drier conditions than sites with moss or sedges.
  - **H2** I expect drier soils on slopes than in flat or hollow areas and I expect the moisture content to decrease with elevation.
- **O3** Quantify how vegetation cover, topography and soil moisture affect soil temperature.
  - **H1** Vegetation cover significantly influences summer soil temperatures, e.g. I expect cooling effects under lichen and mosses due to albedo and insulation effects, but the strongest cooling effects I expect due to shadowing under shrub canopies.
  - **H2** Soil moisture significantly influences summer soil temperatures. I expect lower temperatures at sites with high soil moisture due to evaporative cooling (in the wind blown valley).
  - **H3** Topography significantly influences summer soil temperatures. I expect warmer soils in locations less exposed locations (hollows, depressions).

2 STUDY AREA

The study site is in Blæsedalen (*Itinneq Kangilleq*), a valley located in the south of Disko Island (*Quequertarsuaq*), Western Greenland, approximately 3km northeast of the port and town of Quequertarsuaq and the University of Copenhagen's Arctic Station (`http://arktiskstation.ku.dk/english/`) (Fig. 2). The area lies within the discontinuous permafrost zone, active layers typically remain frozen from October to late May (Xu et al., 2021; D'Imperio et al., 2017).

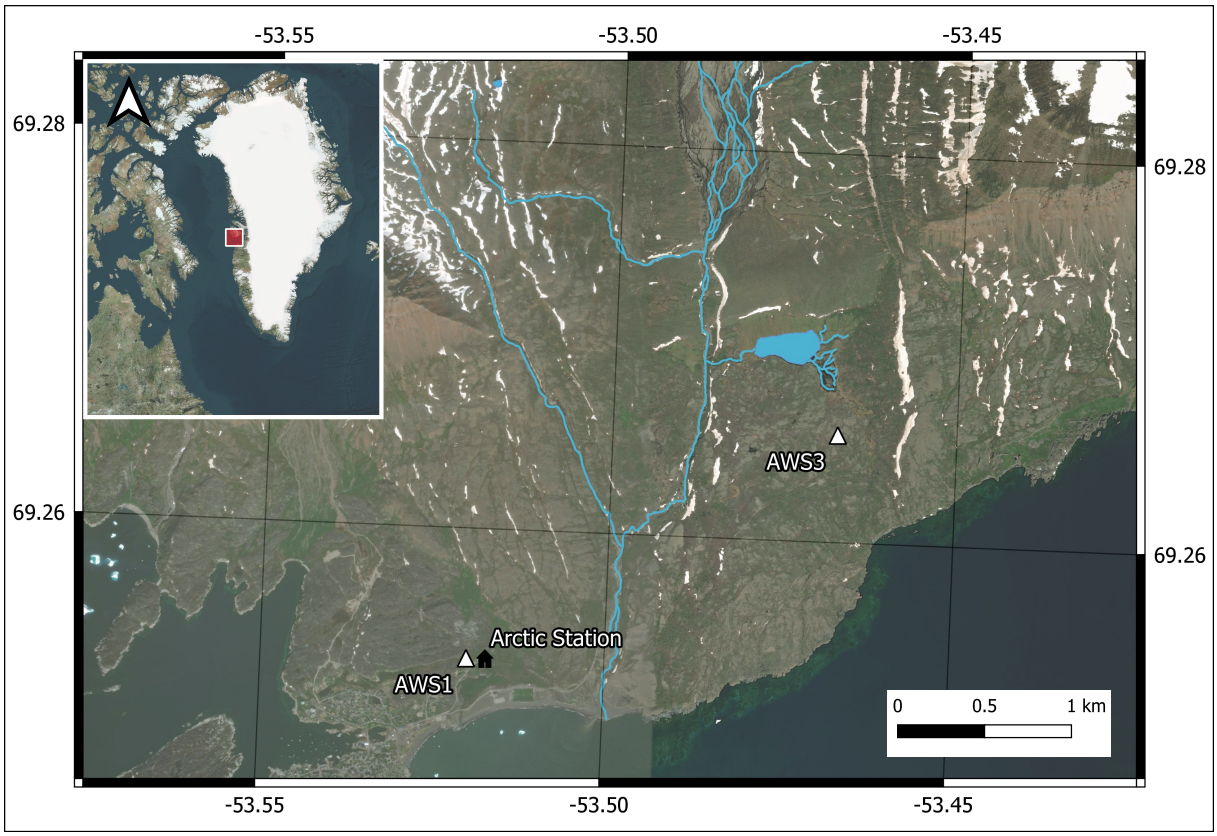

Figure 2: Blæsedalen in the south of Qeqertarsuaq (Disko Island), Western Greenland with study area (white rectangle), automatic weather stations 1 and 3 (AWS1, AWS3) operated by the Greenland Ecosystem Monitoring programme and Arctic station. Hydrological features: Von Oppen et al. (2022). Basemap: Microsoft, Bing Maps, accessed 2024. (`http://ecn.t3.tiles.virtualearth.net/tiles/a{q}.jpeg?g=1`)

2.1 Climate

Disko Island is located within bio-climatic sub-zone D of the Arctic tundra, characterized by a maritime Arctic climate. Annual and summer (Jun-Aug) mean temperatures in the study area from 1991–2017 were -3 ± 1.8 °C and 6.8 ± 1.3 °C (mean ± SD), respectively.

Mean annual precipitation during the same period was 418 ± 131 mm yr^{-1} (mean ± SD), with roughly 65% accounting for liquid precipitation (Zhang et al., 2019). From 1991 to 2004, the mean annual soil temperature at 5 cm depth was -0.9℃ (Hansen et al., 2006; Hollesen et al., 2015). Effects of climate change at the study site have been documented in long term climate observations: Zhang et al. (2019) identified a warming trend in air temperatures from 1991 to 2005, with increased inter-annual variation in more recent years (2006-2017). Over the entire study period (1991-2017), a consistent trend of a lengthening growing period was observed, characterized by an increasing number of days with minimum soil temperatures above 0℃. As for precipitation, the mean value during the period 2008-2017 decreased by roughly 25% compared to the 1991-2008. The transition to a drier and warmer climate is linked to shifts in species composition: (Callaghan et al., 2011) observed shrub establishment and a shift from fell-field to heath at sites in Blæsedalen between 1967 and 2009. (Hollesen et al., 2015) attributed rising summer and winter temperatures to increased growth of deciduous dwarf shrub *Betula Nana* as an indication of Arctic greening.

2.2 Vegetation

Bio-climatic sub-zone D of the Arctic tundra exhibits relatively high vegetation cover and diversity, compared to other Arctic sub-zones. Vegetation cover ranges from 5-50% in dry areas to 80-100% in moist areas. Typical vegetation includes non-tussock sedges, dwarf-shrubs and mosses (Raynolds et al., 2019; Walker et al., 2005; Hansen et al., 2006). According to the Circumpolar Arctic Vegetation Map by Raynolds et al. (2019), the vegetation at the study site is classified as 'erect dwarf shrub and moss tundra (S1)', where plant communities are dominated by dwarf shrubs with less then 40 cm in height, growing on moist to dry acidic soils. Von Oppen et al. (2022) describe the vegetation as dense, consisting of low, erect dwarf-shrubs mixed with herbaceous plants, mosses, and lichen. Dominant shrub species at the study site include deciduous dwarf shrubs (*Salix Glauca*, *Vaccinum Uliginosum*, *Betula Nana*) and evergreen low shrubs (*Cassiope Tetragona*, *Empetrum Nigrum*.

3 METHODOLOGY

3.1 Study Design

To study the links between vegetation cover, topography, soil moisture and temperature I used data obtained at the study site during multiple field campaigns between September 2022 and September 2024 (Boike et al., 2024). Data acquisition was conducted along two transects on the eastern slope of the valley (Fig. 3). Due to their uphill orientation, both transects span an elevation gradient from 85 m a.s.l. near the valley floor to 110 m a.s.l. on the eastern slope. Each transect crosses four visually identified vegetation units. Per vegetation unit, three sites of 1 m^2 size (plots in the following) were chosen, totaling in 24 plots (Fig. 4). Plots at lower elevations within vegetation unit E on transect 1 are located in flat terrain in close proximity to a lake, where wetlands are present. Plot 16-18 exhibited saturated conditions with visible water-tables during the field campaign (Fig. 21, Section A.2). The location of the transects and plots were chosen by an expert to ensure a representative coverage of the vegetation types in the valley and to account for within-unit variability.

3.2 Data Sets

Temperature-Moisture Sensors

A TOMST TMS-4 temperature-moisture sensor (TMS sensor) (Wild et al., 2019) is placed at the center of each plot (Tab. 2, Section A.1). They provide temperature at three heights and are designed to resemble the scale of a small herbaceous plant: Canopy height (+15 cm), near surface (+2 cm) and ground (-6 cm). For the purpose of this study I only used data provided by the sensor measuring soil temperature at 6 cm depth. The lower part of the TMS sensor contains a moisture sensor using the time-domain transmission method (TDT) to provide the soil moisture within the upper 15 cm of the ground. The TMS sensors recorded at 15-minute intervals, beginning with the installation on September 7–8, 2022, and continuing until the most recent data retrieval on September 11 - 19, 2024. The sensors measure temperature with a resolution of 0.0625 °C and with an accuracy of ± 0.5 °C (which was increased to ± 0.3 °C after ice-bath calibration, see Section 3.5).

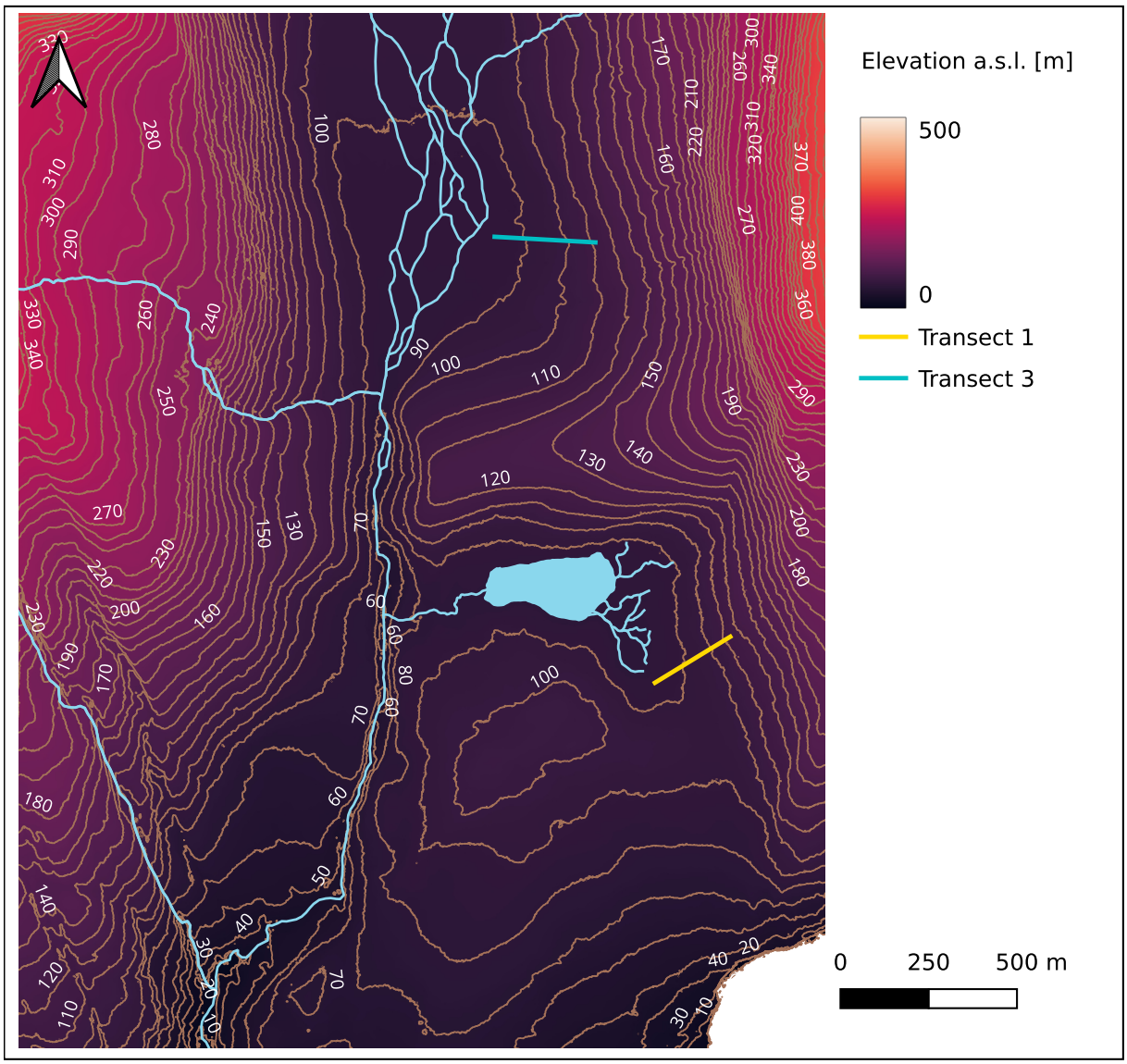

Figure 3: Topographic map of the study area. Transects 1 and 3 are located on the eastern slope of Blæsedalen in the South of Qeqertarsuaq (Disko Island), Western Greenland. Hydrological features: Von Oppen et al. (2022). DTM License: Based on material by Maxar Products. `GRL_Qeqertarsuaq_0m50_L1_DTM_001_EGM96.tif` © 2024 Maxar Technologies, including material by AW3D Enhanced, AW3D Metro, AW3D Standard and AW3D Telecom Products. `GRL_Qeqertarsuaq_0m50_L1_DTM_001_EGM96.tif` © 2024 NTT Data Corporation and by Ecopia Building Footprints Powered by Maxar. Ecopia Building Footprints © 2024 Ecopia Tech Corporation. Imagery © 2024 Maxar Technologies, provided by BKG and BMI, all rights reserved.

Soil Moisture at Installation

Two additional soil moisture measurements were taken at installation of the TMS sensors: Soil moisture was measured at each plot using a handheld HydroSense device (Campbell Scientific Ltd.) with an accuracy of 3% and a range of 0-50% volumetric soil moisture (`https://www.campbellsci.de/hs2`). The device measures soil moisture using time-domain reflectometry (TDR), which relies on the same underlying principle of electromag-

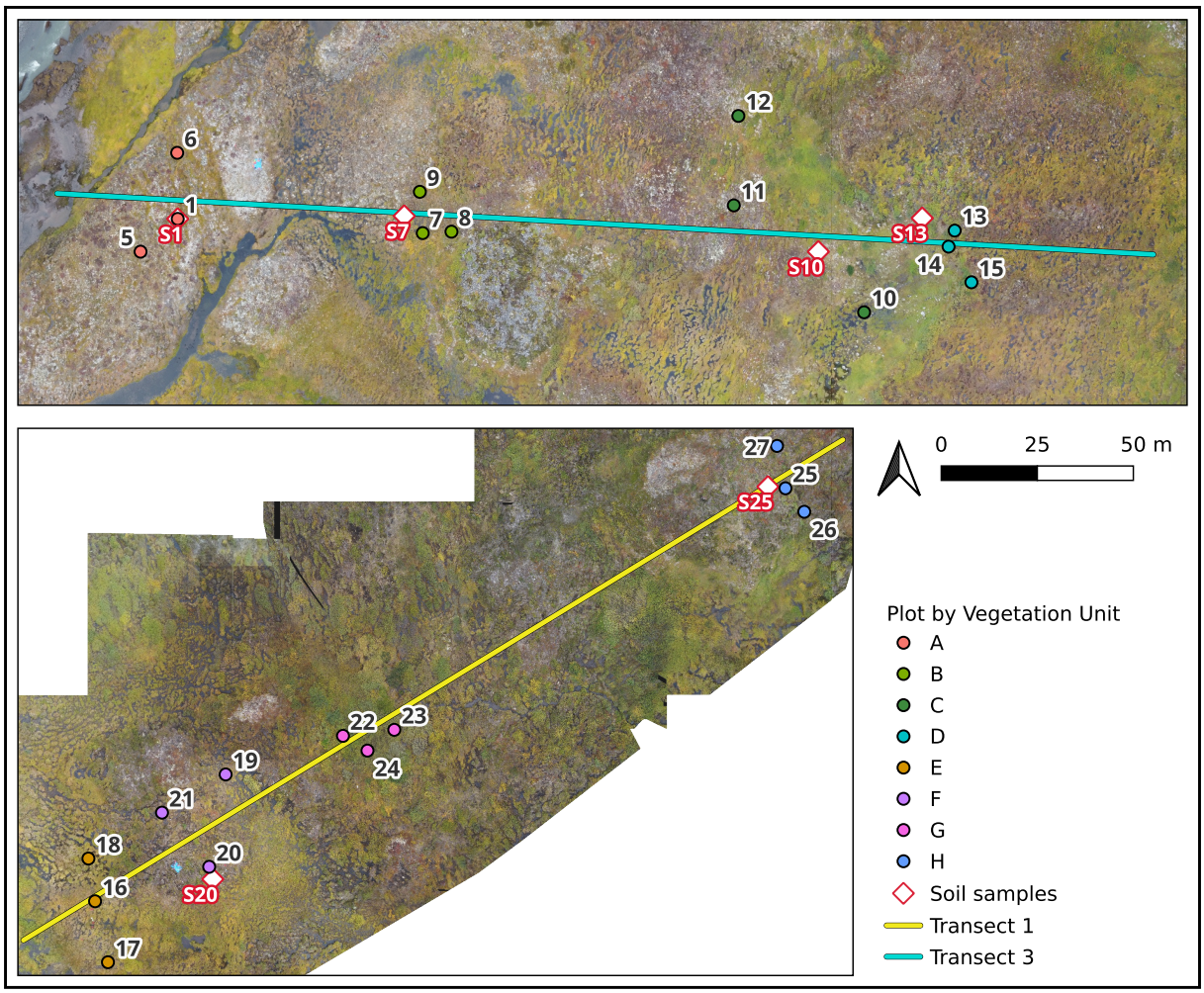

Figure 4: Temperature-moisture sensor locations by vegetation unit along transects 1 and 3 in Blæsedalen in the South of Qeqertarsuaq (Disko Island), Western Greenland. Soil sample locations are named after closest temperature-moisture sensor. Drone-derived ortho-images taken on September 8, 2022 (lower) and September 7, 2022 (upper) in the background (Boike et al., 2024).

netic pulse propagation as the TMS sensors. Second, soil samples were taken within the vegetation units to determine volumetric water content in the laboratory (Fig. 4 and Tab. 3, Section A.1.2). Both measurements were used to verify the TMS sensor soil moisture measurements. Further details on the verification are provided in the data processing section (Section 3.5) and in the Appendix (Section A.1.1, Section A.1.2).

Vegetation Survey

Vegetation composition and height were assessed twice, in September 2022 and September 2023 (Boike et al., 2024). Cover percentage of the most abundant vegetation cover types was observed within the surrounding square-meter of each sensor. Additionally, vegetation height was measured at four fixed positions within each plot according to the

standardized permafrost monitoring protocol (Boike et al., 2021).

Digital Terrain Model

For my terrain analysis, I used a digital terrain model (DTM) with a horizontal resolution of 0.5 m, provided by the Federal Agency for Cartography and Geodesy's Satellite-Based Crisis and Situation Service (*Bundesamt für Kartographie und Geodäsie (BKG), Satellitengestützter Krisen- und Lagedienst (SKD)*) (Fig. 3). The DTM was derived from WorldView-3 optical satellite imagery in stereo configuration using the Semi-Global Matching photogrammetric algorithm developed by the German Aerospace Center (*Deutsches Zentrum für Luft- und Raumfahrt*). Image geometry was refined with 243 tie points to improve relative alignment. The native accuracy of the WorldView-3 data, specified by the provider, is < 3.5 m vertically and < 5 m horizontally. Ground-point masks were applied to distinguish terrain from surface features like vegetation and buildings, which were removed and interpolated to generate the final DTM.

Local Climate Data

Lastly, I used local climate data provided by the local automatic weather stations (AWS, Fig. 2) operated by the Greenland Ecosystem Monitoring Program (`g-e-m.dk`). Air temperature and precipitation have been recorded since 1991 until 2013 by AWS1 (Greenland Ecosystem Monitoring, 2024b) located at the Arctic station and since 2013, air temperature and precipitation are recorded by AWS3, which is located further northeast (Greenland Ecosystem Monitoring, 2024a). Air temperature at AWS1 was measured at 9.5 m and precipitation at 2 m height. Air temperature at AWS3 was measured at 2.2 m height, and precipitation at 0.8 m height with a heated precipitation gauge.

3.3 Study Period

This study focuses on the links between vegetation, topography, soil moisture and temperature in summer. I defined the summer season based on soil temperatures, as TMS sensor moisture measurements are valid only when soil temperatures exceed 0 ℃ (liquid water state). Despite varying freeze and thaw timings of the plots due to local conditions (e.g. snow cover duration), I chose a consistent study period for all sensors to avoid distortion of seasonal mean temperatures due to differences in prevailing weather conditions (Fig. 5).

For each respective sensor I calculated the date when soil temperatures first exceeded 0.3℃ for 10 consecutive days (thawing) and the date when they first fell below 0.3℃ for 10 consecutive days (freezing), using 0.3℃ as a threshold based on TMS sensor accuracy after calibration. The latest thawing and earliest freezing dates across all plots were chosen as start and end of the study period to ensure unfrozen conditions for all soils. The TMS sensor data ends on September 11, 2024, before the 2024 summer season concluded (Tab. 6, Section A.4). While the 2023 season end date (September 20) suggests minimal missing data, I used the 2024 data solely to compare inter-annual variation. My primary analysis focuses on the full 2023 summer period.

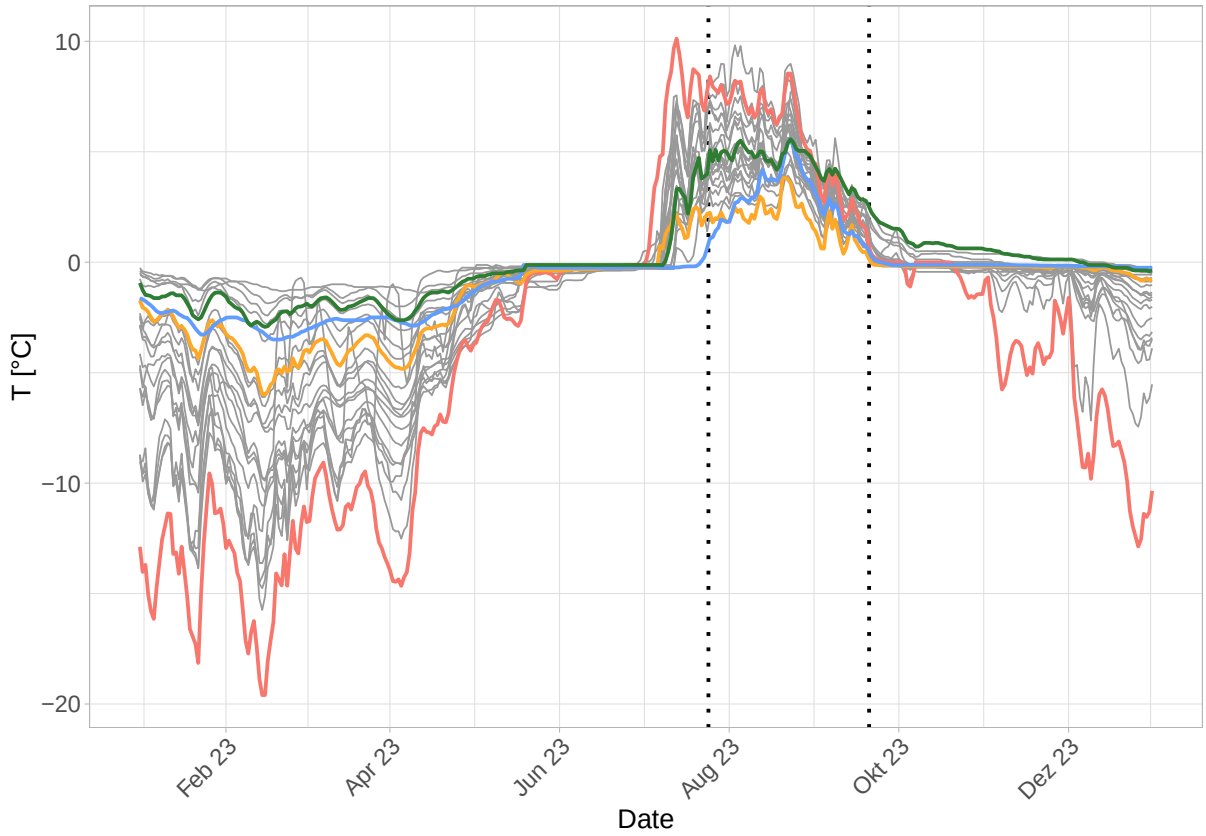

Figure 5: Soil temperature at 6 cm depth recorded in the study area by 23 temperature-moisture sensors during 2023. The temperature graphs illustrate the variations in freeze-thaw timings of the soil across the study area. Dotted lines show beginning and end of study period (summer), limited by latest soil thawing date and earliest freezing date: July 24 to September 20, 2023. Highlighted time series show plots with: *Red* - Earliest thawing date (at plot ID 1), *Blue* - Latest thawing date (at plot ID 12), *Orange* - Earliest freezing date (at plot ID 7), *Green* - Latest freezing date (at plot ID 24).

3.4 Pre-Processing of the TMS Sensor Data

All processing steps (if not mentioned otherwise) and the analysis were performed in R Studio using R version 4.1.0 (R Core Team, 2021).

Cleaning the Data

Out of the 24 TMS sensors, the ones at plot 9 and 17 (Fig. 4) broke within the first year after installation and were replaced in September 2023. The data of sensor 17, however, was later retrieved and the time series of the two sensors were merged, leaving only 2 days of no data. The raw temperature and moisture measurements of all sensors were then processed using R Studio (R Core Team, 2021) and the *myClim* package (Man et al., 2023). First, all observations preceding the first valid moisture signal after installation were excluded based on the time at which each sensor recorded stable moisture values exceeding zero (Grünberg et al., 2020). Next, I removed invalid values where the sensor had itself set an Error-flag and, after visual inspection, excluded observations where moisture measurements dropped below 100.

Calibration of Soil Temperatures

The soil temperature measurements were calibrated with values from an ice-bath calibration. Before installation, all sensors were held into an ice-bath at 0℃. After short time, the temperature sensors reached an equilibrium temperature, reflecting the sensor specific measurement error. I corrected the raw temperature data by subtracting the respective measurement errors, resulting in a calibrated temperature time series, which was then used for further analysis (Fig. 15, Section A.1).

Conversion of Raw Soil Moisture Measurements

The raw soil moisture measurements collected by the TMS sensors utilize the time-domain transmission method, which involves sending electromagnetic pulses through the ground to assess soil moisture levels. The raw values of the TMS sensors represent the frequency of received pulses, which correlates with the soil's moisture content. Transmission based measurement techniques like TDT depend on soil specific parameters such as bulk density and organic matter content and hence require calibration (Wild et al., 2019). The signal

can be translated to soil moisture (given as the volumetric water content (VWC)), using a parametrized conversion formula dependent on the soil type (Wild et al., 2019). Kopeckỳ et al. (2021) created a universal conversion formula (eq. 1, Section A.1.1) for unknown soil types by repeating the calibration protocol from Wild et al. (2019) for different soil types and combining them into one parametrization. The formula is implemented into the *myClim* package in R (R Core Team, 2021) by the authors and I applied it to the raw soil moisture measurements (Fig. 18). Due to the simplified assumptions of the universal conversion formula, the resulting soil moisture values potentially underestimate the soil moisture in organic soils and overestimate it in certain mineral soils (Section A.1.1).

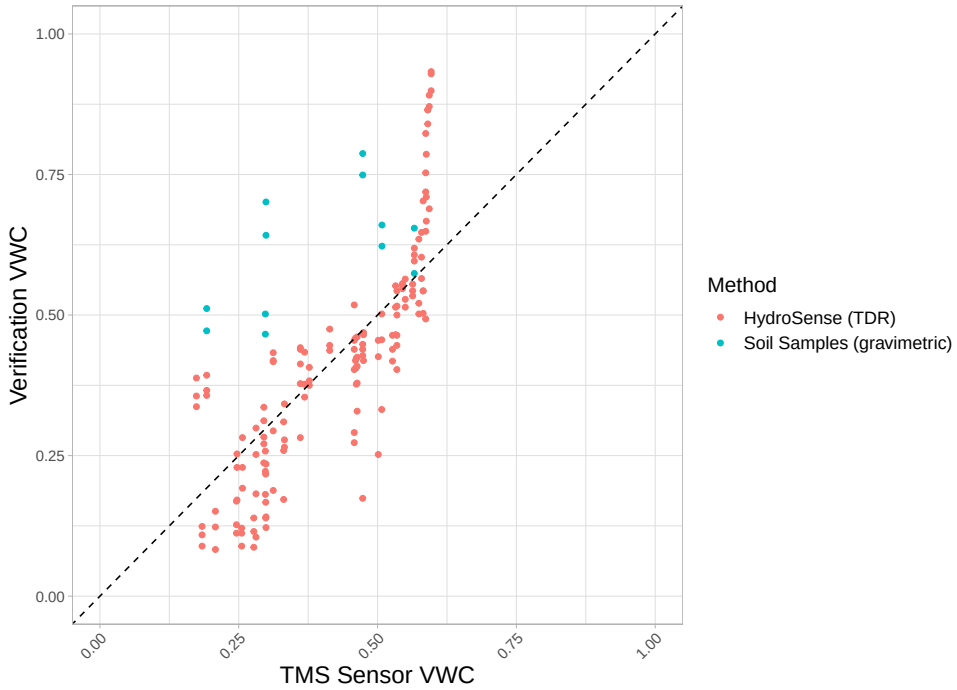

Figure 6: Comparison of three measurement methods for soil moisture given as volumetric water content (VWC) within the upper soil (0 - 15 cm) for verification of the temperature-moisture sensor data. X-Axis: Soil moisture values recorded by temperature-moisture sensors located in the study area after installation (September 8 - 11, 2023). Y-Axis: *red* - Soil moisture recorded with a HydroSense II (Campbell Scientific Ltd.) using time-domain reflectometry (TDR) at each plot, *blue* - soil moisture derived from soil samples located within the vegetation unit of the corresponding sensor (see Fig. 4 for sample locations). Dashed line is identity line.

Verification of Soil Moisture Values

In order to verify the TMS sensor soil moisture measurements, I compared them with HydroSense measurements taken at installation and soil moisture derived from soil samples (gravimetric) (Fig. 6). For the comparison, the soil sample and HydroSense measurements

were matched up with the TMS measurement closest in time (Fig. 19, Section A.1.2). The deviation of HydroSense measurements from the TMS sensor measurements is -0.01 ± 0.12 (mean ± sd), whereas measurements more than 5% above the range given by the manufacturer (0 - 50%) tend to be higher than TMS measurements and measurements within the range tend to be lower than TMS measurements. Within the advised value range of the HydroSense, the deviation increases to -0.04 ± 0.09 (mean ± sd). The deviation of gravimetric soil moisture measurements from TMS sensor measurements is 0.22 ± 0.12 (mean ± sd).

3.5 Variable Construction

Before starting my main analysis, I aggregated the data sets from different sources to derive variables representing vegetation cover, topography, soil moisture and temperature of the plots (Tab. 1).

Soil Temperature		
meanT	Mean soil temperature during summer	[℃]
Soil Moisture		
meanMoist	Mean soil moisture during summer	[%]
Vegetation		
vegHeight	Averaged vegetation height	[cm]
vegDens	Vegetation density	-
Forbs	Forb cover	[%]
Graminoids	Graminoid cover	[%]
Lichen	Lichen cover	[%]
Moss	Moss cover	[%]
Shrubs	Shrub cover	[%]
Topography		
elevation	Elevation above sea level	[m]
geomorphon	Terrain feature type according to geomorphons	-
slope	Terrain steepness	[°]

Table 1: Variable Overview. Soil temperature and moisture variables derived from temperature-moisture sensor data obtained in the study area between September 2022 and September 2024 for the respective summer seasons of 2023 and 2024. Vegetation variables were derived from vegetation height and species cover within the 1 m^2 plots surrounding the temperature-moisture sensors during field campaigns September 2022 and September 2023. Species cover values were summarized by their respective plant functional type. Topographic parameters derived from a digital terrain model using terrain analysis tools implemented in QGIS (QGIS Development Team, 2019) and the geomorphon approach to landform classification (Stepinski and Jasiewicz, 2011).

Soil Moisture and Temperature

After cleaning and calibrating the soil temperature and moisture data provided by the TMS sensor, I calculated the seasonal mean soil temperature and mean soil moisture per plot for the respective summer seasons of 2023 and 2024.

Vegetation Cover and Height

Vegetation height and cover percentage of the most common cover types were assessed in 2022 and 2023 for every plot (Section 3.2). First, I calculated mean vegetation height from the eight respective measurements per plot (Fig. 20, Section A.2). For vegetation cover, I filtered out the least common cover types with less than 50% overall occurrence ($< 0.5\ m^2$), resulting in nine main vegetation types (Fig. 23, Section A.2). Next, I classified them by their plant functional types (PFT, Tab. 4, Section A.2). Using plant functional types to classify tundra vegetation species depending on their grow form is widely adapted, as species of the same PFT exhibit similar responses to and effects on ecosystem changes ((Chapin III et al., 1996). Typical PFTs found in the Arctic tundra are mosses, lichen, graminoids, forbs and shrubs (evergreen and deciduous). I summed up the respective cover percentages of the PFTs per each plot (Fig. 24, Section A.2). As a proxy for vegetation density, I accumulated cover percentages of the PFTs shrubs, graminoids, forbs and moss (all except for lichen due to its low density).

I averaged the observations for each respective sensor location over the two years to increase the robustness of the observations. I chose this approach to enhance statistical power by increasing the number of observations. Given that vegetation community changes in Arctic tundra ecosystems typically occur gradually and not within a single year, this averaging method provides a more representative measure of vegetation structure since the differences between the two observations are more likely to be rooted in the subjectivity of the visual cover percentage assessment and the within-plot plant height variation.

Topography

For each plot, I extracted elevation directly from the DEM (Section 3.2) and calculated the slope using the terrain analysis tool included in QGIS (QGIS Development Team, 2019). I then categorized the landscape into feature types using the geomorphons concept as proposed by Stepinski and Jasiewicz (2011). The parameter-based pattern recognition

algorithm is used to classify a landscape into common topographic features such as summit, slope or depression. A detailed description of the method, my parameter choices and the resulting landscape classification are provided in Section A.3. Due to the location of the transects, only two geomorphon classes are represented in my data: hollow/footslope and slope.

3.6 Statistical Analysis

To quantify summer soil moisture and soil temperature variation within plots and seasons, and explore the relationships between vegetation cover, topography, soil moisture and temperature I used statistical measures (mean, standard deviation) and linear regression models.

I calculated the respective mean values for soil temperature and soil moisture in summer, including standard deviation, to visualize spatial and temporal variation on the plot level.

To quantify the links between the plant functional cover types, vegetation height and density, elevation, slope, landform and mean summer soil moisture, I computed single linear regression models for each variable as a predictor with moisture as the response and extracted the significance level (*p-value*) and amount of explained variance (R^2). Beforehand, I visualized predictor and response distributions, calculated the spatial autocorrelation of the moisture and temperature data (Section A.6) and checked all predictor variables for collinearity. I calculated Pearson's R for all variable pairs to visualize them in a correlation matrix. To check model assumptions and quality of the results I created residual- and quantile-quantile-plots (QQ-plots). Analog to this I quantified the links between the plant functional cover types, vegetation height and density, elevation, slope, landform, mean summer soil moisture and mean summer soil temperature.

4 RESULTS

4.1 Climate Conditions

To understand the underlying climate conditions influencing permafrost soil temperatures, I examined temperature and precipitation patterns, with a primary focus on the summer of 2023 and, for comparative purposes, the summer of 2024. While the data set for 2024 is incomplete (January 1 - September 11, 2024), partial data still allows for an initial comparison. Additionally, placing the seasons in a long-term context shows trends and potential anomalies of the climate conditions during the study period. When comparing the two summer seasons, I only included observations that lie within the overlap of summer seasons 2023 and 2024 (Section A.4).

Precipitation

Annual precipitation totaled 418.2 mm in 2023, with a substantial portion (349.9 mm) falling between January and September. In contrast, the January-September period in 2024 recorded a significantly lower precipitation total of 144.1 mm. The histogram of monthly precipitation (Fig. 7, right panel) highlights the seasonal variation, with 2023 showing a more pronounced summer rainfall peak than 2024. The summer precipitation in 2023 was 150.4 mm, exceeding the 2024 season with 97.4 mm.

During the observation period from 1992 to 2023 (considering only complete years) the mean annual precipitation was 282 mm ± 118 mm with annual precipitation values ranging between 134 mm and 600 mm. The precipitation in 2023 is above the annual average while the precipitation in 2024 so far hints towards the lower range of annual precipitation (Fig. 27, Section A.6.1).

Air Temperature

In 2023, the annual mean air temperature was recorded at -4.4℃, characteristic of the persistently cold conditions typical for Arctic regions. The time series plot (Fig. 7,left panel) illustrates temperature variations over two years (2023-2024), revealing pronounced seasonal fluctuations with distinct peaks and troughs. From January to September 2023, the mean temperature was -4.2℃, lower than the -3.5℃ observed during the same period in

2024. However, the summer of 2023, exhibited a higher mean temperature of 6.4 ℃, compared to 5.6 ℃ in the summer of 2024.

Over the long-term period from 1992 to 2023, the annual mean air temperature averaged -3.2 ℃ ± 1.7 ℃. During this time, the mean annual temperature ranged from 0.97 ℃ in the warmest to -6.69 ℃ during the coldest year. Compared to this period, the annual mean temperatures for both seasons are colder than average but remain within the range of the standard deviation (Fig. 27, Section A.6.1).

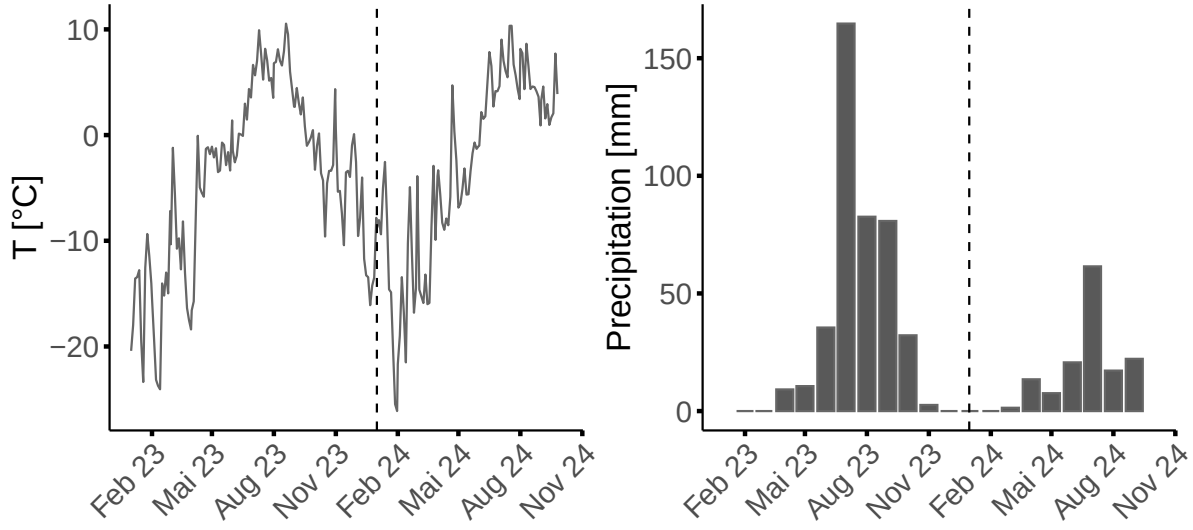

Figure 7: Air temperature at 2.2 m height and liquid precipitation measured with a heated rain gauge by automatic weather station 3 located in the study area. Air temperature measurements are averaged over a 3-day moving window. Precipitation is accumulated to monthly values. Both data sets are complete during the depicted period (no missing data). Dashed line shows beginning of 2024.

4.2 Spatial and Temporal Variation of Soil Temperature and Moisture

I compared summer soil moisture and temperature between plots and across the summer seasons of 2023 and 2024 to quantify the spatial and temporal variation within the plots. The beginning and end date of the respective summer seasons 2023 and 2024 differ. For comparisons between seasons, I only used observations included in the overlapping part of both summer seasons (Section A.4).

Soil Moisture

Summer soil moisture levels differ substantially within the study area: The mean soil moisture varied between 14% and 60% across all plots in summer 2023 (Fig. 8, right panel). Soils on transect 1 generally exhibited higher soil moisture levels (49% ± 11%, mean ± sd) than soils on transect 3 (31% ± 12%, mean ± sd).

Mean soil moisture across all plots was 40% ± 14% in summer 2023 and 37% ± 15% in summer 2024 (Fig. 9). Higher soil moisture in 2023 aligns with higher annual and summer precipitation in 2023 (Section 4.1). In 2024, reduced soil moisture was particularly evident on transect 1. Despite overall seasonal differences, spatial soil moisture patterns were consistent, as shown by observations aligning along the identity in Fig. 9.

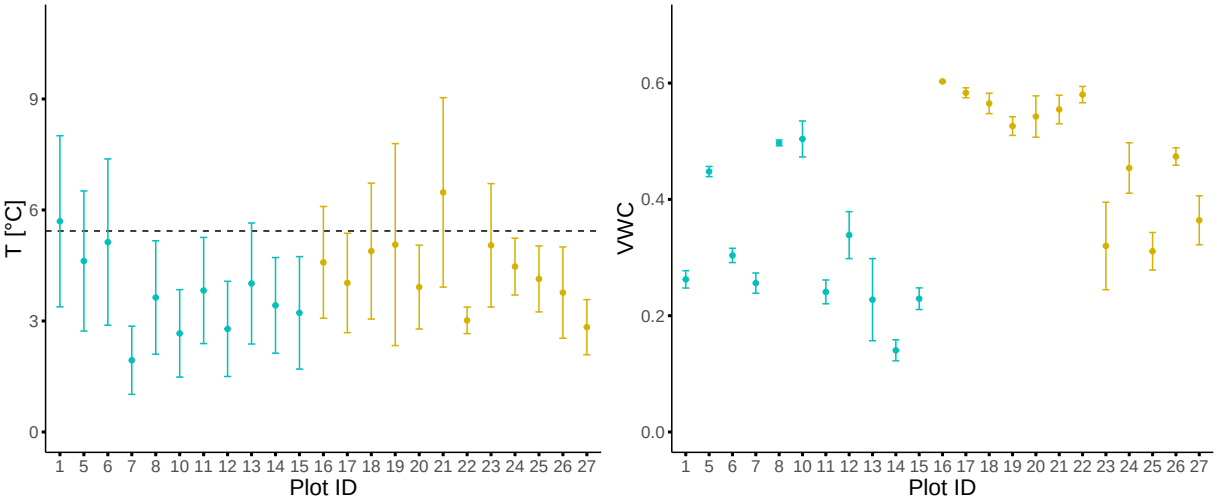

Figure 8: *Left:* Mean soil temperatures with standard deviation at 6 cm depth recorded by temperature-moisture sensors located at 23 plots in the study area during summer season 2023 (Jul 24 - Sep 20). Dashed line shows mean air temperature during summer season 2023. *Right:* Mean soil moisture given as volumetric water content (VWC) of the upper 15 cm recorded by temperature-moisture sensors during summer season 2023. *Yellow:* Transect 1, *Blue:* Transect 3.

Soil Temperature

Despite the spatial proximity of the plots, mean summer soil temperatures ranged between 1.9 ℃ and 6.5 ℃ in 2023. These results illustrate the deviation from the mean summer air temperature of 5.4 ℃ (Fig. 8, left panel). During the season 2023, mean summer soil temperatures on transect 1 were warmer (4.4 ℃ ± 1 ℃, mean ± sd) than those on transect 3 (3.7 ℃ ± 1.1 ℃, mean ± sd).

Mean soil temperatures in 2023 were overall lower compared to 2024 with 4.4 ℃ ± 1.8 ℃ and 4.8 ℃ ± 2 ℃ (mean ±sd) (Fig. 9). This is consistent with a warmer January-September

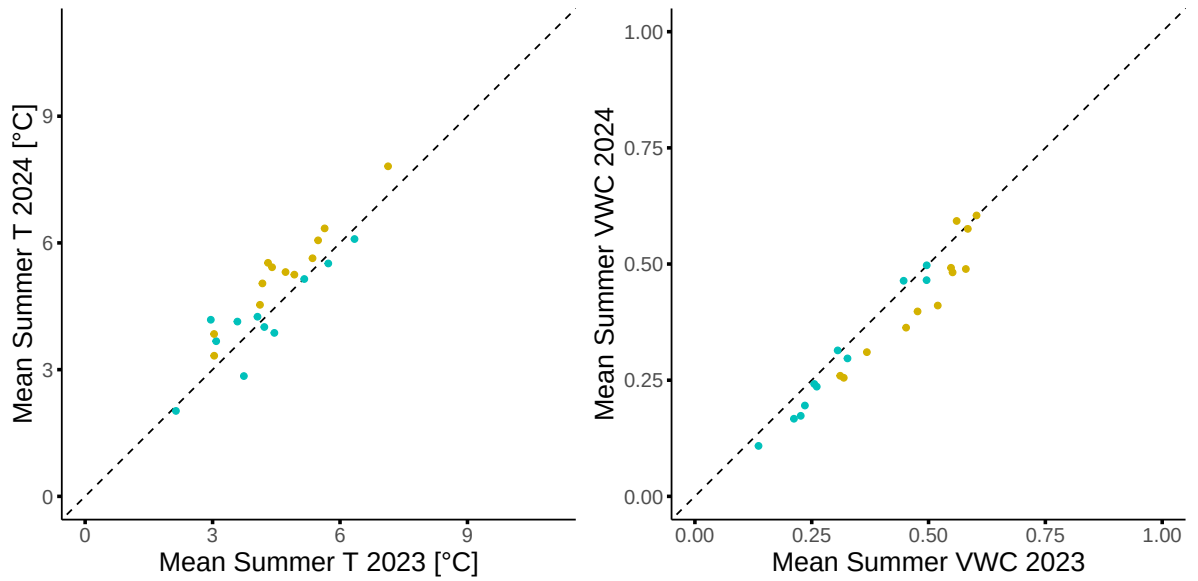

Figure 9: *Left:* Comparison of mean soil temperature at 6 cm depth measured by temperature-moisture sensors during the overlapping period of the summer seasons of 2023 and 2024 (Jul 24 - Sep 11). *Right:* Comparison of mean soil moisture given as volumetric moisture content (VWC) of the upper 15 cm by temperature-moisture sensors during the overlap of summer seasons 2023 and 2024. Dashed line is identity.

period in 2024, but not with the colder temperatures during summer 2024.

4.3 Variable Correlation

To assess the relationships among the vegetation and topographic variables, I computed a correlation matrix. This matrix provides an overview of how these variables interact among each other, which is essential for interpreting results from the single linear models applied in the subsequent analyses.

Collinearity among predictors might indicate that variables share explanatory power or even influence each other. However, correlation analysis is a simplified measure of a linear relationship between two variables and bears no measure of robustness, which is why it is important to gain an understanding of the data the analysis is based on. The variables lichen, forbs and graminoids are distributed unevenly across their total variable range (Fig. 29, Section A.6.3). Specifically, there is an under-representation of plots with high values for the respective cover percentage and slope. Calculating a correlation value for a non representative sub-sample of the total value range can lead to wrong implications and should hence be treated with caution. This is true for correlations among the predictors as well as the linear models build from these variables in Section 4.4 and Section 4.5

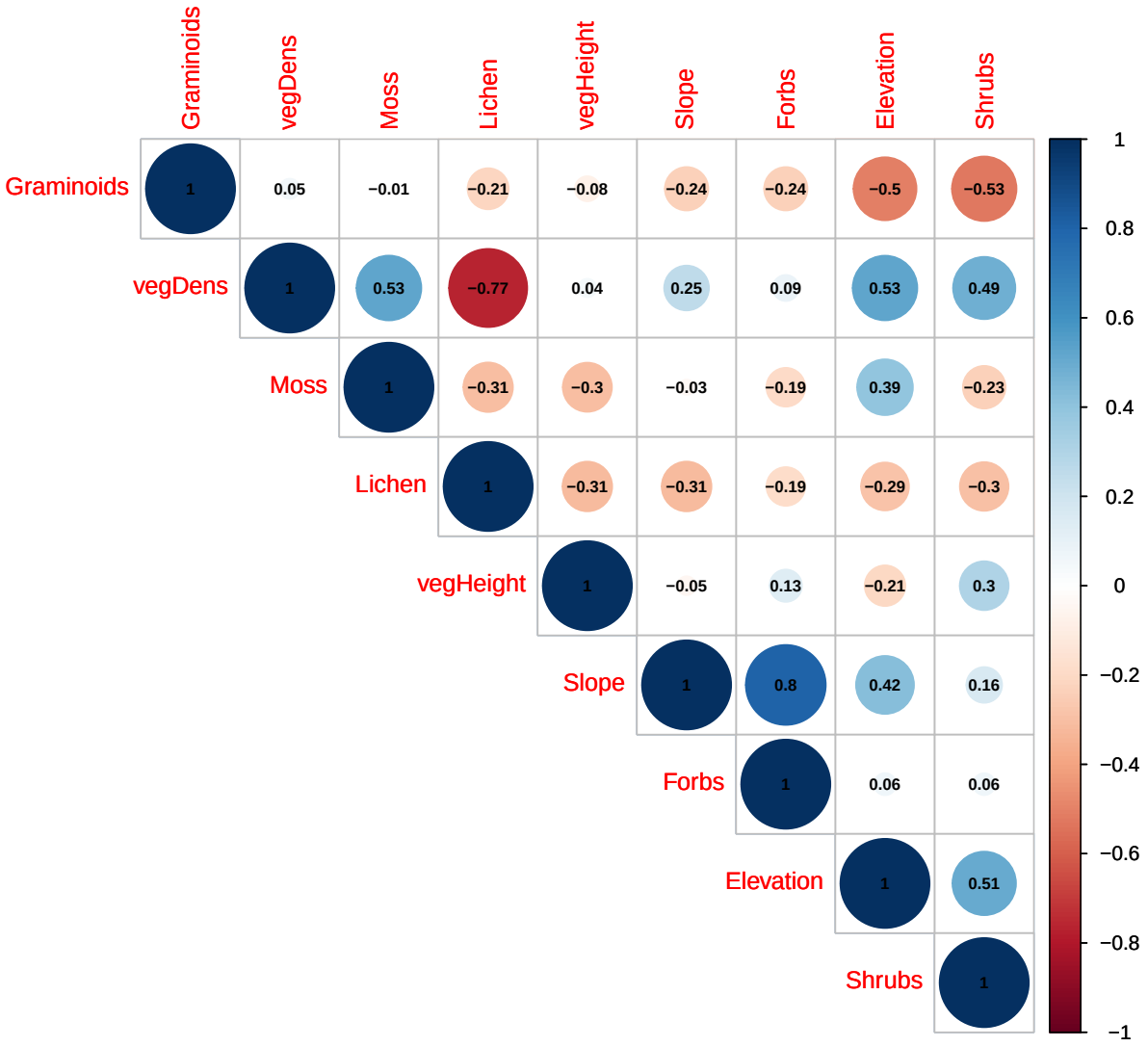

Figure 10: Correlation matrix with Pearson's R computed for all continuous vegetation cover and topography variables. Values near 1 imply strong positive correlation, values near -1 strong negative correlation and 0 implies no observed correlation between two variables.

Upon reviewing the correlation matrix, several notable relationships among the variables emerge. Vegetation density is positively correlated with moss cover (R^2 = 0.53) and shrub cover (R^2 = 0.49), which are both included in the calculation of vegetation density. Vegetation density shows a strongly negative correlation with lichen cover (R^2 = -0.77), possibly reflecting that high vegetation abundance within a plot leaves less room for another species type (lichen) to occur as well or that lichen preferably grows in less vegetated areas within the study area. Lichen is also negatively correlated to moss cover (R^2 = -0.31) indicating that the two ground cover species tend to exclude each others abundance in the plots.

Shrub cover is negatively correlated to graminoid cover (R^2 = -0.53) and lichen cover (R^2 = -0.3), which could reflect differences in their growing conditions. Vegetation height is positively correlated with shrub cover(R^2 = 0.3) and negatively correlated with lichen (R^2 = -0.31) and moss cover (R^2 = -0.3), reflecting their respective heights as well as a potential tendency of the ground cover species to be less associated with abundance of tall growing plants.

The topographic variables slope and elevation (since geomorphon is a categorical variable it is not included in the matrix) are correlated with each other (R^2 = 0.42), confirming that the topographic location of the transects up the eastern slopes of the valley on a landscape scale is, to an extent, consistent with the slope on smaller topographic scales (< 1 m). The correlation matrix additionally reveals a positive correlation between elevation and vegetation density (R^2 = 0.53) as well as elevation and shrub cover (R^2 = 0.51) and elevation is negatively correlated with graminoid cover (R^2 = -0.5).

4.4 How Topography and Vegetation relate to Moisture

To understand the relationship between topography, vegetation cover and summer soil moisture, I analyzed single linear models with mean summer soil moisture as the response and each of my respective topographical and vegetation cover variables as a predictor.

The analysis identified elevation (p = 0.012, R^2 = 0.28), graminoid cover (p = 0.003, R^2 = 0.35) and geomorphon type (p = 0.003, R^2 = 0.35) as significant predictors of soil moisture.

Elevation showed a negative relationship with summer soil moisture, with higher elevations generally exhibiting lower moisture levels. However, the collinearity analysis indicated that elevation also correlates positively with both vegetation density and shrub cover, reflecting potential vegetation cover effects on moisture retention characteristics. Further, the lowest-lying plots on transect 1 are located in flat terrain within the wetlands bordering the lake.

Geomorphon type further emphasizes the influence of topography on moisture distribution with 35% of explained variance in the soil moisture data (Fig. 12). Hollow/footslope areas had significantly higher mean moisture levels with 47.7% ± 12.7% (mean ± sd) soil moisture compared to plots located on slopes which exhibited 31.2% ± 10.3% (mean ± sd) soil moisture content. Since geomorphon type correlates with the other topographic

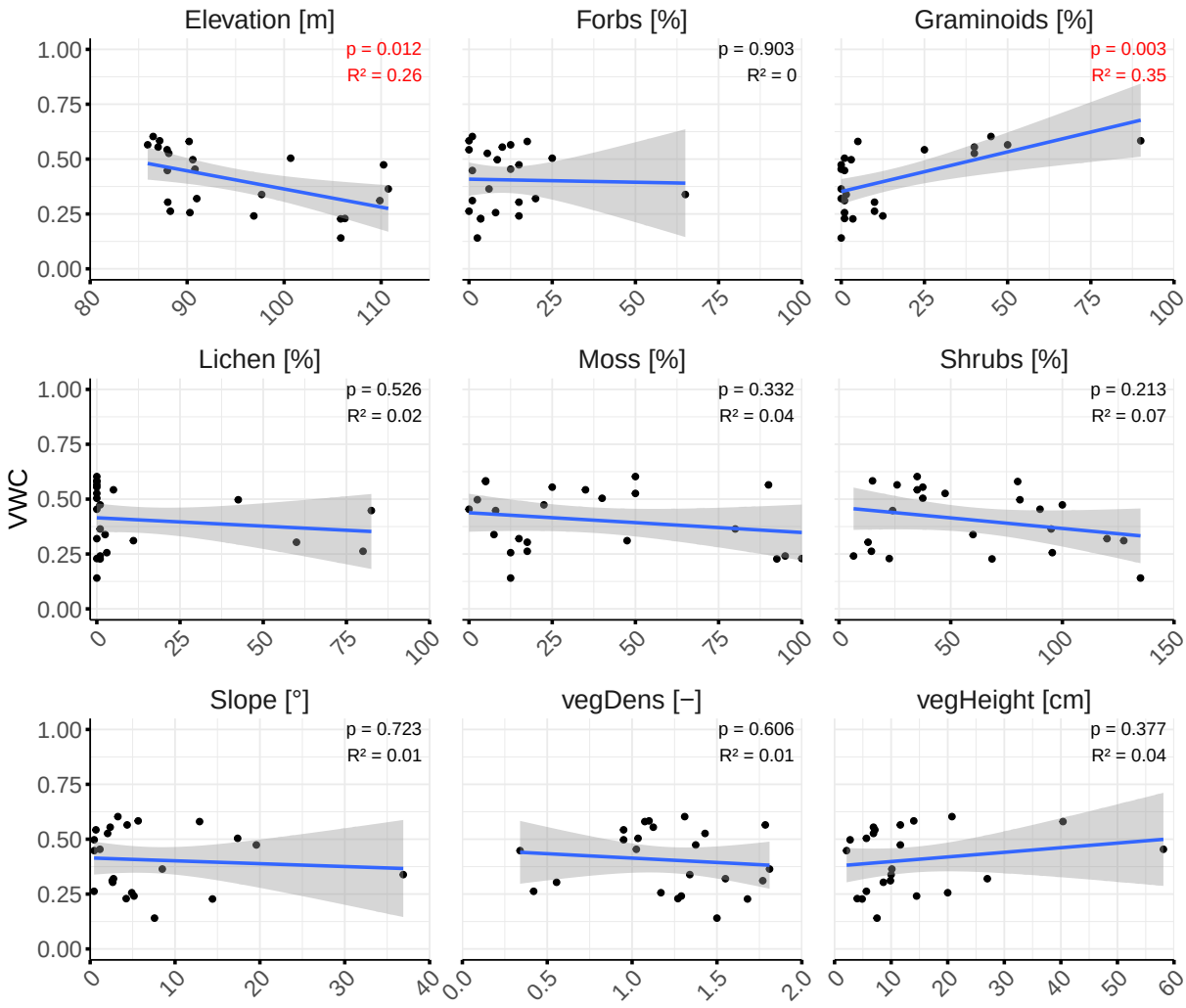

Figure 11: Scatter plots for all vegetation cover and topography variables plotted against mean soil moisture during the summer season 2023 given as volumetric water content (VWC) of the upper soil (0 - 15 cm) with linear regression line (*blue*) and 95% confidence interval. P-values calculated with Fisher's test and explained variance (R^2) of the linear regression are colored red when the relationship is considered significant (p < 0.05).

variables slope and elevation, it is likely that some of the relationship observed between elevation and moisture also reflects underlying geomorphon effects. Slope exhibited a non-significant relationship with soil moisture (p = 0.723, R^2 = 0.01).

As for the vegetation variables, graminoid cover had a positive and significant correlation with soil moisture (p=0.003, R^2 = 0.35). From the collinearity analysis, I observed, that graminoid cover is negatively correlated with shrub cover, which implies that graminoid-dominated areas were more prevalent in open, moist sites, whereas shrubs were more common in relatively drier areas. The correlation analysis also revealed a negative relationship between graminoid cover and elevation, implying that the effect of graminoid cover

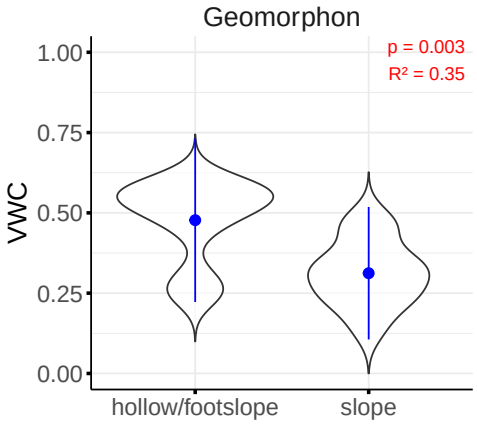

Figure 12: Violin plot of the mean soil moisture given as volumetric water content (VWC) of the upper soil (0 - 15 cm) during summer season 2023 in hollow/footslope and slope areas. With group mean (*blue point*) and standard deviation (*blue line*).

might partly be assigned to elevation.

All other vegetation variables (forbs, lichen, moss and shrubs as well as vegetation density and height) showed no significant linear relationships (Fig. 11). However, the p-value in statistics is a somewhat arbitrary threshold used to assign a binary label of significance to a continuous spectrum of probability. While not significant by definition, the variables for shrub (p = 0.213, R^2 = 0.07) and moss cover (p = 0.332, R^2 = 0.04) both exhibit a non-significant, negative relationship with soil moisture. As do the other vegetation cover variables lichen and forbs, but they and the graminoid cover variable exhibit an uneven distribution (Section A.6.3, Fig. 29) and coverage of the variable range, causing increased uncertainty of the results.

In summary, my analysis revealed that elevation, graminoid cover, and geomorphon type explain most variance in soil moisture levels in the study area. Elevation shows a negative relationship with soil moisture and hollow and footslope geomorphon types retain more moisture than slopes, further highlighting the role of topographic features. Graminoid cover correlates positively with soil moisture, while shrub and moss cover show less pronounced negative relationships with soil moisture.

4.5 How Topography, Vegetation and Moisture relate to Soil Temperature

To explore the factors influencing summer soil temperatures, I examined how vegetation cover, topography and soil moisture individually relate to soil temperature using linear regression models.

The regression analysis (Fig. 14) indicates that elevation and slope were significantly negatively correlated with mean soil temperature (p = 0.021, R^2 = 0.23 and p = 0.015, R^2 = 0.25 respectively) suggesting that higher and steeper areas tend to have cooler soils. Slope alone explains 25% of the variation in soil temperature, underscoring its importance as a topographic predictor in this environment. However, the correlation analysis showed that slope and elevation themselves were positively correlated, meaning that a share of their respective explanatory power might be associated to the other, or that one is masking the effect of the other. Furthermore, both transects are positioned along an elevational gradient and cover a similar range of elevation values (Section 3.1). Thus, elevation may serve as a proxy for spatial proximity of the observation points on the transect level. The comparison of soil temperature between the geomorphon types hollow/footslope and slope adds additional context: While mean soil temperature does not significantly differ between these types (p = 0.689, R^2 = 0.01), there is a broader temperature range within hollow/footslope areas, suggesting greater variability in these topographic settings.

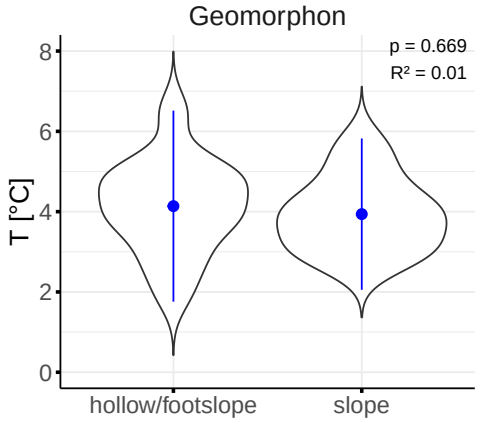

Figure 13: Violin plot of the mean soil temperature during summer season 2023 in hollow/footslope and slope areas. With group mean (*blue point*) and standard deviation (*blue line*).

The vegetation cover variables only exhibited non-significant relationships with soil tem-

perature (Fig. 14). Graminoid cover explained most variance in the data and showed a positive association (p = 0.07, R^2 = 0.15). The correlation matrix revealed a negative correlation between graminoid cover and elevation that potentially caused elevation effects to be masked by graminoid cover within this comparably small sample.

Following graminoids, lichen cover explained 12% of variance in the data (p=0.104) and is positively associated with soil temperatures while forb cover and shrub cover both exhibited a negative relationship with summer mean temperatures (R^2 = 0.08, p = 0.19 and R^2 = 0.01, p = 0.132, respectively). Moss cover showed no evident effect on mean summer soil temperatures (p = 0.828, R^2 = 0). Vegetation density and vegetation height both exhibited non-significant, negative relationships with mean summer soil temperature (p = 0.279, R^2 = 0.06 and p = 0.793, R^2 = 0, respectively).

Soil moisture showed a positive but non-significant correlation with soil temperature (p = 0.311, R^2 = 0.05).

In summary, slope and elevation were key factors affecting summer soil temperature, with higher and steeper areas tending to be cooler. Slope alone explained 25% of temperature variation, underscoring its importance. Although summer soil temperature doesn't significantly differ between geomorphon types, hollow/footslope areas show greater temperature variability. Vegetation types mostly show non-significant associations with soil temperature, graminoid cover was most important and is positively correlated to soil temperature. Soil moisture is marginally positively correlated with soil temperature.

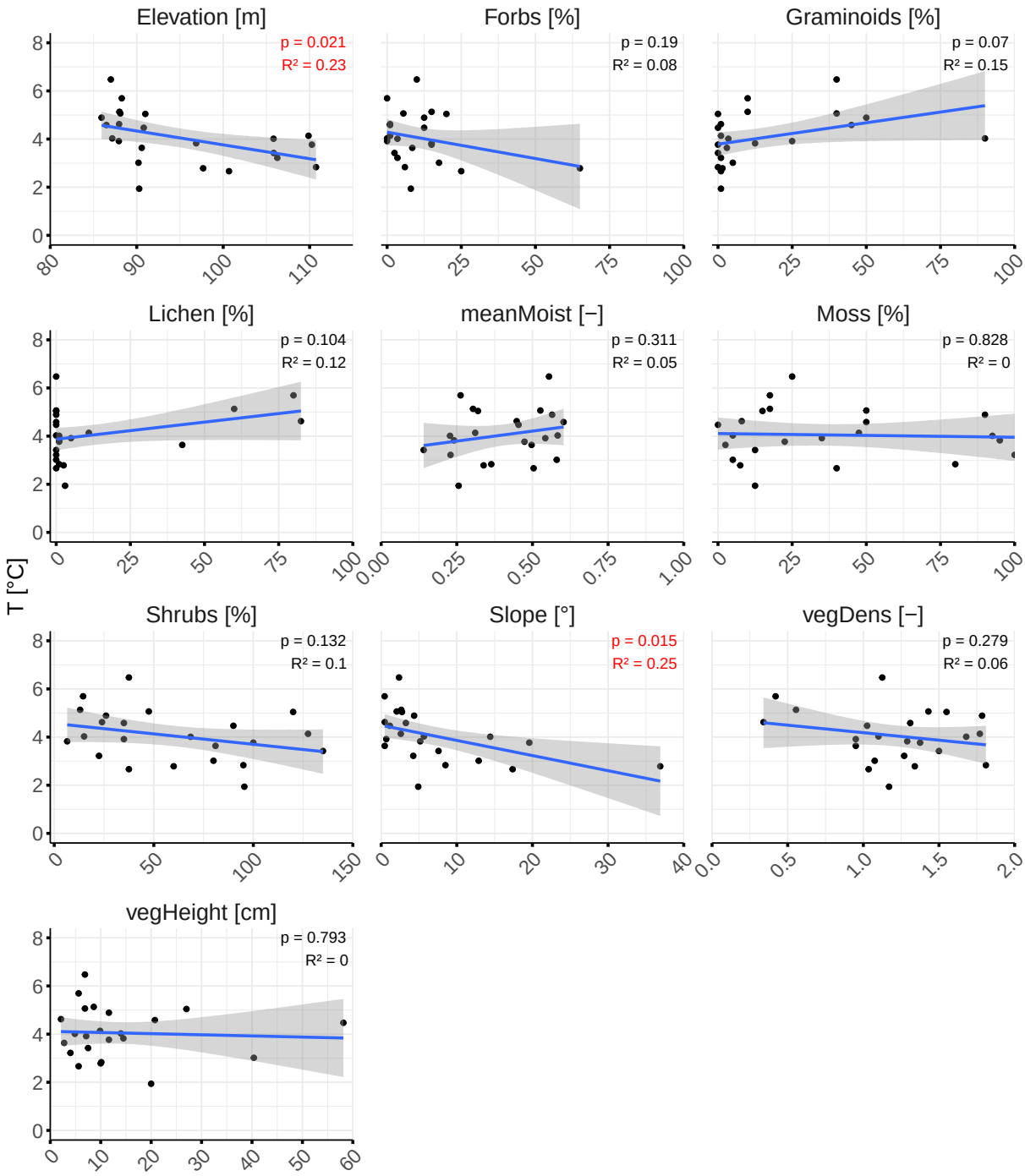

Figure 14: Scatter plots for all vegetation cover, topography and soil moisture variables plotted against mean soil temperature during the summer season 2023 with linear regression line (*blue*) and 95% confidence interval. P-values calculated with Fisher's test and explained variance (R^2) of the linear regression are colored red when the relationship is considered significant (p<0.05).

5 DISCUSSION

In this thesis, I studied the links between vegetation, topography, and soil moisture and their influence on small-scale soil temperature variation during summer at Blæsedalen, a valley in the south of Disko Island, Western Greenland. For this purpose, I focused my analysis on time-series data collected during the summer season of 2023 using TMS sensors at 24 locations. The locations differ in vegetation composition and moisture regimes and are placed along an elevational gradient with increasing elevation and steepness. Using field observations and a digital elevation model, I derived descriptive variables to quantify vegetation cover and height, topography, soil moisture, and soil temperature for each location. I then used linear regression analysis to compare their explanatory power. The results indicate that the distinct patterns of summer soil moisture and the deviations of soil temperature from the local air temperature observed in the study area mostly associated with the topographical characteristics of the landscape.

5.1 TMS Moisture Data Verification

To verify results of the conversion of raw TMS sensor measurements to soil moisture, gravimetric soil moisture and HydroSense derived soil moisture were used as a reference. Gravimetric measurements were consistently higher than those obtained from transmission-based methods (TDR in HydroSense and TDT in TMS sensors), with a difference in soil moisture of 22% ± 12% (mean ± sd). HydroSense and TMS sensor soil moisture, which rely on similar measurement principles, differed less from each other with a mean soil moisture difference of 4% ± 9% (mean ± sd) within the advised value range.

A wide range of soil moisture sensors is available, many of which can effectively capture soil moisture dynamics and responses to local weather conditions. However, their absolute values can differ significantly, especially when not calibrated to the specific site conditions (Jackisch et al., 2020). The universal formula provided by Kopeckỳ et al. (2021) is useful to derive soil moisture values from soils with unknown parameters and has been applied to capture value ranges of different soils including peat soils where the conversion formula provided by Wild et al. (2019) yielded unrealistic values (Kemppinen et al., 2023). However, the differences between TDT and gravimetric soil moisture measurements possibly reflect this lack of on-site calibration. Further, gravimetric measurements of soil moisture can gen-

erally exhibit higher values because they measure both free and hygroscopically bound water, opposed to transmission based methods. While the smaller mean absolute difference between TDT and TDR measurements and the diminished standard deviation reflect the similarity of the method, the remaining differences can be rooted in differences in raw value conversion: User controlled signal conversion is possible for the TMS sensors, but the signal is internally converted with an unknown conversion formula in the HydroSense.

Overall, the observed TMS sensor soil moisture values align with findings from other studies of surface soil moisture in Arctic tundra regions (Kemppinen et al., 2023; Von Oppen et al., 2022). Despite the general underestimation of moisture content by the TMS sensors, their relative consistency with TDR measurements suggests they are suitable for inter-plot comparisons. Future research should include on-site calibration of soil moisture sensors to improve absolute accuracy and ensure comparability.

5.2 Climate Conditions

In 2023, precipitation totaled 418.2 mm, exceeding the long-term annual mean of 282 mm, while 2024 recorded significantly lower precipitation. Annual mean air temperatures for both years were colder than the long-term average (-3.2 ℃ ± 1.7 ℃, mean ± sd), with 2023 (-4.4 ℃) and 2024 (-3.5 ℃) showing typical seasonal variation but remaining within historical variability. While these results not necessarily reflect the overarching shift towards a warmer climate, the differences in precipitation represent the increasing annual variability in the study region observed by Zhang et al. (2019).

5.3 Spatial and Temporal Variation of Soil Moisture and Temperature

In summer 2023, soil moisture levels varied significantly across the study area, with mean volumetric water content (VWC) ranging from 14% to 60%. This aligns with the higher precipitation in 2023, as the soil moisture levels in 2024 were generally lower, particularly on transect 1. Mean summer soil temperatures in 2023 ranged between 1.9 ℃ and 6.5 ℃ and were generally lower (4.4 ℃ ± 1.8 ℃, mean ± sd) compared to 2024 (4.8 ℃ ± 2 ℃, mean ± sd), which correlates with the warmer temperatures in 2024 during the January-September period, but not during the cooler summer months.

The results agree with observations of high summer soil moisture and temperature variability on small spatial scales caused by the heterogeneity of tundra landscapes (Aalto et al.,

2013, 2022). Spatial variability of summer soil temperature and moisture exceeds seasonal variability, and their respective value ranges align with other observations of tundra summer soil moisture (Kemppinen et al., 2023).

This result underlines again that local climate variables alone are not sufficient to describe small scale soil moisture and temperature patterns without taking location characteristics (e.g. vegetation, topography) into account.

5.4 Topography and Vegetation Effects on Soil Moisture

The analysis of the relationship between topography, vegetation, and summer soil moisture identified geomorphon type (R^2 = 0.35), graminoid cover (R^2 = 0.35), and elevation (R^2 = 0.28) as most important predictors of soil moisture. Moisture levels in the study area decrease with increasing elevation and analog, soils in hollows or at footslopes exhibit higher moisture levels than on slopes, while graminoid cover showed a positive correlation with moisture. Other vegetation variables, including shrub (R^2 = 0.07) and moss cover (R^2 = 0.04), demonstrated weaker relationships with soil moisture.

5.4.1 Topography

Geomorphon type was the strongest predictor of soil moisture, explaining 35% of variance in the data, followed by elevation (R^2 = 0.28). Slope exhibited no relationship with soil moisture (R^2 = 0.019. The increased soil moisture at lower elevation and in more sheltered locations aligns with expected patterns of soil moisture drainage and distribution. Kemppinen et al. (2023) highlighted the strong spatial variability of soil moisture in tundra environments, emphasizing that topographic variations significantly affect moisture conditions. Additionally, wind exposure and the maximum incoming solar radiation are controlled by topographic factors. They influence snow accumulation patterns, which in turn affect soil moisture levels (Zhang, 2005; Sundstøl and Odland, 2017; Penna et al., 2009). Besides water availability, soil moisture mainly is related to texture and porosity, which determine the moisture retention capacities of the ground (Legates et al., 2011). These properties are found in organic horizons rather than in mineral, which agrees with findings by (Petters et al., 2024), who sampled soil moisture at three locations in the study area. Plots 16-22 on transect 1 exhibit a volumetric water content of around 60% throughout the whole observation period with only little variation (low standard deviation). Moisture values of this range

are typically found in organic horizons due to their physical properties and potentially reflect the increased organic matter content of the wetland plots in hollow/footslope areas at lower elevation of transect 1.

5.4.2 Vegetation

Of all vegetation variables, graminoid cover could account for most variance in the moisture levels (R^2 = 0.35) and is positively correlated with summer soil moisture levels. The other vegetation cover variables shrubs, moss, forbs, lichen and vegetation density exhibited non significant negative relationships with soil moisture, besides vegetation height which showed a positively correlation.

Graminoids

Graminoids were the most important vegetation cover variable (R^2 = 0.35). They grow in both wet and moderately dry soils, making them resilient to changes in water availability. Under wet conditions, graminoids can dominate the landscape following permafrost thaw, while they may be outcompeted by shrubs under drier conditions (van der Kolk et al., 2016). The positive association between graminoid cover and soil moisture in my results may reflect these vegetation responses to permafrost degradation processes in the study area. Reversely, dense graminoid cover can enhance soil moisture retention. Arctic plant species follow different strategies for nutrient uptake, expressed in the morphology of their root system. Chen et al. (2020) compared root traits of typical Arctic shrub and graminoid species and found graminoids to have finer and more branched root systems, creating finer pores and limiting hydraulic within soil water movement (Scholl et al., 2014). However, graminoids - as well as lichen and forbs - exhibit uneven coverage of the value range with an underrepresentation of plots exceeding 20% cover area of the respective cover types (Fig. 29, Section A.6.3). Graminoids also correlate with shrub cover (R=-0.53) and elevation (R=-0.5). Both limits statistical power of my results and potentially causes graminoid cover to mask effects of other variables. Compared to other plant types such as shrubs and mosses, there is limited research on the interactions between graminoids and soil moisture in Arctic ecosystems. My results, along with their increasing significance under changing climate conditions, suggest that graminoids should be given greater attention in future studies concerning surface soil moisture in the Arctic tundra, especially at sites with high graminoid coverage.

Shrubs

Shrub cover is negatively related to soil moisture in the study area. Drier soil conditions favor shrub growth on one side (van der Kolk et al., 2016), and dense shrub cover in return increases evapotranspiration and intercepts with precipitation, also leading to decreased moisture levels in the the upper soil layer (Bonfils et al., 2012; Zwieback et al., 2019; Kemppinen et al., 2021). Additionally, thick shrub root systems can lead to reduced moisture retention (Chen et al., 2020; Scholl et al., 2014). To further investigate the effects of shrub cover in summer, especially the height-dependent effects (e.g. shadow), a more detailed approach to vegetation classification could improve the results (Sulman et al., 2021). While the classification into five plant functional types was suitable for my comparatively small sample, distinguishing between low and tall shrubs allows for a better capture of important plant-traits (Sulman et al., 2021).

Moss

High moss coverage is non-significantly associated with drier soils. Generally, the effects of moss on the soil thermal and hydrological regime are closely related to the thickness of the moss mat (Gornall et al., 2007; Schuuring et al., 2024). Gornall et al. (2007) found, that soil under thicker moss layers was drier than under thin moss cover, potentially reflecting moisture losses due to precipitation interception or due to the insulating effect of moss layers, which can offset summer thawing of the ground, thus preventing meltwater infiltration into the ground (Hinzman et al., 1991). However, Gornall et al. (2007) also argue, that moss layers can buffer moisture losses in the underlying soil due to decreased evaporation and disjointed moisture transfer between the upper moss layer and the soil (Miller et al., 1980). A combination of opposing effects arising from several different processes can cause an overall low correlation. Additionally, moss cover at the study site is positively correlated with elevation, so potential positive effects on soil moisture under thick moss over may be overpowered by strong elevation effects.

Vegetation Height and Density

While high vegetation density can increase the evapotranspiration and thereby lead to drier conditions (Horton and Hart, 1998), vegetation has also been reported to increase soil moisture levels due to shadow effects under high vegetation that reduce evaporative losses (Daly and Porporato, 2005; Asbjornsen et al., 2011). Further, roots systems can create a

finer pore structure and limit soil water movement, thus enhancing soil moisture retention (Scholl et al., 2014). In the study area, vegetation density tends to increase with elevation, implicating that potential positive effects of dense vegetation cover on moisture content might be overpowered by topographic effects.

5.5 Topography, Vegetation and Soil Moisture Effects on Soil Temperature

The analysis of the relationship between topography, vegetation cover, summer soil moisture and summer soil temperatures revealed that slope (R^2 = 0.25) and elevation (R^2 = 0.23) were the most significant factors influencing summer soil temperature, with higher and steeper areas exhibiting cooler soils. Vegetation cover produced only non significant correlations, with graminoid cover (R^2 = 0.15) and lichen (R^2 = 0.12) exhibiting the strongest positive association with soil temperature. Soil moisture also showed a marginal positive correlation (R^2 = 0.05) with soil temperature.

5.5.1 Topography

Slope and elevation were overall the most important predictors for summer soil temperature (R^2 = 0.25 and R^2 = 0.23), while geomorphon type had no significant relationship and could only explain 1% of variance in the data. Higher elevations and steeper slopes typically experience greater wind exposure (Sundstøl and Odland, 2017) and more efficient drainage, which can lead to reduced heat retention in soils due to lower heat capacity. Topography also controls exposure to incoming energy, the orientation and inclination of slopes determine the amount of maximum solar radiation received by the soil. Von Oppen et al. (2022) have identified incoming solar radiation as one of the most important factors for daily mean temperatures during summer in the same study area. South-facing slopes generally experience higher temperatures, while north-facing slopes remain cooler, a trend that is especially pronounced in the Arctic due to the low sun angle (Aalto et al., 2018; Aartsma et al., 2023). Small scale variability of incoming solar radiation within the geomorphon classes due to varying slope angles could explain the comparably low influence of the landform class. This also possibly explains why soils on transect 1, which is on the west-south-facing slope of the valley south of a ridge between the both transects (Fig. 3) exhibit warmer soils than transect 3, which is on the west-north-facing slope north of the ridge.

5.5.2 Vegetation

While none of the vegetation cover variables showed a significant relationship with summer soil temperature, graminoid cover could account for most variance in summer soil moisture levels (R^2 = 0.15) and is positively correlated. The vegetation cover variables shrubs, forbs and vegetation density exhibited non-significant negative relationships with soil temperature, lichen had a positive relationship with summer soil temperature and moss and vegetation height both showed no visible effect on summer soil temperatures.

Graminoids

Graminoid cover accounts for the most variance in soil temperature data (R^2 = 0.15) among all vegetation variables. Graminoids are associated with higher summer soil temperatures, consistent with findings by (Schuuring et al., 2024), who reported that graminoids provide less insulation compared to mosses and shrubs during the growing season. Conversely, graminoid-dominated sites may reflect prior permafrost degradation and thaw, which are linked to warmer soil temperatures and increased moisture levels (van der Kolk et al., 2016). However, the interpretability of these results is limited by uneven variable coverage across the full range of values and correlations with shrub cover and elevation, as noted in Section 5.4.2. Overall, little research has focused on the soil temperature implications of dense graminoid cover in the Arctic. Given recent findings suggesting that graminoids may become increasingly dominant in Arctic tundra ecosystems, further study of their effects on soil temperatures is essential.

Shrubs

Shrub cover has a non-significant negative relationship with soil temperature, reflecting expected canopy shadowing effects (Blok et al., 2010; Frost et al., 2018; Von Oppen et al., 2022). Further, shrubs can cool summer soils due to increased evapotranspiration (Pearson et al., 2013), which may cause reduced thermal conductivity in underlying moss and organic layers which lowers the heat transfer into the ground (O'Donnell et al., 2009). This effect has been observed in a study by (Juszak et al., 2016), who report decreased heat conductivity and shallower active layers under Arctic shrubs compared to wet sedges. (Von Oppen et al., 2022) reported a more pronounced cooling effect of shrub cover on summer soil temperatures in a recent study carried out in the same valley and identified shrub cover (among vegetation height, moss cover and solar radiation) as one of the most important

variables for daily mean temperatures (beside free air temperatures). The comparably lower effect of shrub cover on soil temperatures in my study may arise from dwarf shrubs and tall shrubs both being classified as 'shrub'. This is expressed in the low correlation between shrub cover and vegetation height (R = 0.3). A more differentiated classification may reveal stronger effects of tall shrubs, as noted in Section 5.4.2.

Lichen

Lichen cover is positively related with summer soil temperatures in the study area. While lichen exhibits albedo cooling effects in comparison to bare soil (Stoy et al., 2012), here, the plots with low lichen cover have other vegetation cover. Hence, they experience other warming and cooling effects e.g. through shading or albedo effects. Compared to those plots, high lichen cover is associated with higher soil temperatures. Plots 1,5 and 6 on transect 3 are the only plots with high lichen cover percentage (Fig. 24), which is why lichen may work as a proxy for other site specific factors: The absence of leafy vegetation, for example, may slow down the formation of an insulating organic layer (or indicate it).

Moss

While my results show no association of moss cover and summer soil temperatures, a number of studies have reported the insulating effects of moss cover in the growing season that can reduce soil temperatures and delay summer permafrost thaw (Gornall et al., 2007; Beringer et al., 2001; Van der Wal and Brooker, 2004; Schuuring et al., 2024). An important control on the insulation effect is thickness of the moss layer. Moss represents a physical barrier to incoming radiation and effectively insulates soil due to its low thermal conductivity (Hinzman et al., 1991; Beringer et al., 2001). However, high moisture content of the moss layer increases its heat conductivity and heat capacity (Hinzman et al., 1991; Soudzilovskaia et al., 2013), thereby storing increased amounts of incoming radiation energy and promoting increased evaporative cooling in the growing season (Blok et al., 2011; Jaroszynska et al., 2023) but also potentially increasing heat transfer to underlying soil layers. The weak association here may be a result of a combination of opposing effects, thin moss layers or undetected interactions with moisture.

Vegetation Height and Density

My results suggest that summer soils are cooler under denser vegetation cover. Generally, vegetation acts as a physical barrier which insulates the ground from air temperatures

(Grünberg et al., 2020; Oehri et al., 2022; Heijmans et al., 2022). Increased cooling effects with increased plant height due to e.g. shadowing under tall shrubs are not visible in the data, but plant species taller than 20 cm are barely covered by the data.

5.5.3 Soil Moisture

Contrary to my expectations, that increased soil moisture levels would lower soil temperature due to increased evaporative heat losses in the wind-blown valley, soil moisture exhibited a non-significant positive relationship with summer soil temperatures. Moisture content of the ground affects its thermal conductivity, increasing the heat flux into the soil and thereby altering soil temperature (Heijmans et al., 2022). These ground heat fluxes can be substantial in wet tundra systems (Beringer et al., 2005), but may be altered by extending shrub cover in the future. Dry conditions arising from transpirative moisture transfer to the atmosphere and canopy rainfall interception at shrub sites (Kemppinen et al., 2021; Domine et al., 2016; Zwieback et al., 2019) can lower soil thermal conductivity, thus diminishing the ground heat flux (Loranty et al., 2018).

5.6 Implications under Climate Change

The changing climate directly increases temperatures and alters precipitation patterns in the Arctic, which leads to shifts in species composition and vegetation cover (Tape et al., 2006; Epstein et al., 2012; Bao et al., 2022; Grimes et al., 2024). Simulations by van der Kolk et al. (2016) e.g. predict climate change driven increases in shrub cover at dry sites and in graminoid cover under wet soil conditions. The predicted changes may already be reflected in the observed vegetation distribution in this study, where graminoid cover was positively and shrub cover negatively correlated with soil moisture.

While increased shrub cover has been associated with cooler summer soil temperatures (Blok et al., 2010; Aartsma et al., 2023), the observed warming effects in winter (Myers-Smith and Hik, 2013; Frost et al., 2018; Von Oppen et al., 2022) can overpower the summer warming effects on annual timescales (Heijmans et al., 2022). Increases in graminoid cover may be associated to preceding permafrost thaw, but especially communities of wet sedges can further promote warming of the soil due to increased heat conductivity and lower shading compared to shrubs (Juszak et al., 2016). The effects of vegetation changes on soil temperatures and their association to soil moisture levels in turn have global implica-

tions on greenhouse gas emission, thereby potentially driving positive feedbacks on climate change.

During the summer months, Arctic ecosystems can act as net sinks due to increased plant growth and photosynthesis (Virkkala et al., 2023). However, the growing season is also characterized by enhanced microbial activity and decomposition of organic matter as permafrost thaws, leading to increased carbon and methane release (Schuur et al., 2015; Rößger et al., 2022). While warmer soil temperatures are generally associated with increased microbial activity and greenhouse gas (GHG) emissions, communities of wet sedges, for example, exhibited exhibited higher rates of carbon uptake compared to drier tundra areas (Curasi et al., 2016). However, enhanced carbon sequestration under wet conditions is accompanied by and increase in methane emissions (Virkkala et al., 2023; Donateo et al., 2024). Additional moisture limitations under dry conditions can hinder plant productivity and hence reduce carbon uptake despite warming trends (Zona et al., 2023). To conclude, the expansion of graminoids in the study area, driven by permafrost degradation and increasing soil moisture in poorly drained areas may contribute to further soil warming, but also enhance carbon storage, while potentially increasing methane emissions at the same time. Shrub increases in drier areas may lower annual permafrost soil temperatures due to shadowing effects, but dry soil conditions can limit plant carbon uptake and increase carbon release. These implications underline the importance of vegetation-moisture-temperature relationship for the global climate, as the balance between greenhouse gas sequestration and emission leads to either positive of negative feedbacks on climate change.

5.7 Outlook

For future research, several improvements can be made to enhance the robustness and applicability of findings. First, ensuring that sensor calibration accurately reflects site conditions is crucial, as proper calibration forms the foundation for reliable measurements and enables better comparability with other studies. Increasing the sample size and covering the full range of vegetation classes, particularly graminoids and other under-represented vegetation types in this study, will provide a more comprehensive understanding of their ecological effects. Additionally, refining the vegetation classification to distinguish between tall and dwarf shrubs will more accurately reflect the key characteristics of vegetation cover.

Expanding the sample size or increasing temporal resolution, utilizing the dense time series provided by TMS sensors, would also enable the investigation of interactions between variables over time. Lastly, higher temporal variability would facilitate analysis of the ecosystem's response to extreme weather events, adding valuable insights into how these systems react to short-term climate fluctuations.

6 CONCLUSION

This thesis has explored the relationships between vegetation cover, topography, and soil moisture and their individual influence on small-scale soil surface temperature and moisture variations during the summer months in Blæsedalen, Disko Island, Western Greenland. The findings highlight that topographical features, particularly elevation, slope and landform, are significant determinants of summer soil moisture and temperature dynamics. Specifically, lower elevations and sheltered locations exhibit higher moisture levels, while steeper slopes and higher elevations correlate with cooler soil temperatures due to increased exposure and efficient drainage.

The analysis further revealed that out of all vegetation variables, graminoid cover was most influential, which may be an artifact of under-representation of high coverage sites. Nonetheless, graminoids show potential of enhancing soil moisture retention and can serve as indicators of moisture availability following permafrost degradation. In contrast, shrub cover is negatively associated with soil moisture levels, likely due to increased evapotranspiration and precipitation interception. Moss coverage shows weak correlations with drier soils, but generally plays a central role in moderating evaporation and insulating the soil in Arctic ecosystems. Contrary to expectations, soil moisture was only weakly associated with warmer soils, due to increased heat conductivity.

Overall, the results underscore the importance of considering both vegetation composition and topographic characteristics when assessing soil temperature and moisture patterns in Arctic tundra ecosystems. The study contributes insights into how these factors interact under changing climate conditions, emphasizing the need for further research on graminoids and their ecological significance in Arctic landscapes. This understanding is crucial for predicting future changes in tundra ecosystems as they respond to ongoing climatic shifts. Further, the alteration of temperature-moisture patterns affects greenhouse gas emissions in Arctic ecosystems. Hence, understanding vegetation-temperature-moisture interactions is central to estimate the potential feedbacks on climate change.

REFERENCES

J. Aalto, P. C. le Roux, and M. Luoto. Vegetation mediates soil temperature and moisture in arctic-alpine environments. *Arctic, Antarctic, and Alpine Research*, 45(4):429–439, 2013.

J. Aalto, D. Scherrer, J. Lenoir, A. Guisan, and M. Luoto. Biogeophysical controls on soil-atmosphere thermal differences: implications on warming arctic ecosystems. *Environmental Research Letters*, 13(7):074003, 2018.

J. Aalto, V. Tyystjärvi, P. Niittynen, J. Kemppinen, T. Rissanen, H. Gregow, and M. Luoto. Microclimate temperature variations from boreal forests to the tundra. *Agricultural and Forest Meteorology*, 323:109037, 2022.

P. Aartsma, A. Odland, S. Reinhardt, and H. Renssen. Drivers of soil temperature variation in alpine lichen heaths and shrub vegetation during the summer. *Arctic, Antarctic, and Alpine Research*, 55(1):2209397, 2023.

AMAP. Key trends and impacts. summary for policy-makers. *Arctic Monitoring and Assessment Programme (AMAP)*, 16, 2021.

H. Asbjornsen, G. R. Goldsmith, M. S. Alvarado-Barrientos, K. Rebel, F. P. Van Osch, M. Rietkerk, J. Chen, S. Gotsch, C. Tobon, D. R. Geissert, et al. Ecohydrological advances and applications in plant–water relations research: a review. *Journal of Plant Ecology*, 4 (1-2):3–22, 2011.

T. Bao, G. Jia, and X. Xu. Warming enhances dominance of vascular plants over cryptogams across northern wetlands. *Global Change Biology*, 28(13):4097–4109, 2022.

J. Beringer, A. H. Lynch, F. S. Chapin, M. Mack, and G. B. Bonan. The representation of arctic soils in the land surface model: the importance of mosses. *Journal of Climate*, 14 (15):3324–3335, 2001.

J. Beringer, F. S. Chapin III, C. C. Thompson, and A. D. McGuire. Surface energy exchanges along a tundra-forest transition and feedbacks to climate. *Agricultural and Forest Meteorology*, 131(3-4):143–161, 2005.

B. K. Biskaborn, S. L. Smith, J. Noetzli, H. Matthes, G. Vieira, D. A. Streletskiy, P. Schoeneich, V. E. Romanovsky, A. G. Lewkowicz, A. Abramov, et al. Permafrost is warming at a global scale. *Nature communications*, 10(1):264, 2019.

R. Bivand and G. Piras. *spdep: Spatial Dependence: Weighting Schemes, Statistics and Models*, 2023. URL `https://CRAN.R-project.org/package=spdep`. R package version 1.2-8.

A. D. Bjorkman, I. H. Myers-Smith, S. C. Elmendorf, S. Normand, N. Rüger, P. S. Beck, A. Blach-Overgaard, D. Blok, J. H. C. Cornelissen, B. C. Forbes, et al. Plant functional trait change across a warming tundra biome. *Nature*, 562(7725):57–62, 2018.

D. Blok, M. M. Heijmans, G. SCHAEPMAN-STRUB, A. Kononov, T. Maximov, and F. Berendse. Shrub expansion may reduce summer permafrost thaw in siberian tundra. *Global Change Biology*, 16(4):1296–1305, 2010.

D. Blok, M. Heijmans, G. Schaepman-Strub, J. van Ruijven, F.-J. W. Parmentier, T. Maximov, and F. Berendse. The cooling capacity of mosses: controls on water and energy fluxes in a siberian tundra site. *Ecosystems*, 14:1055–1065, 2011.

J. Boike, S. Chadburn, J. Martin, S. Zwieback, I. H. Althuizen, N. Anselm, L. Cai, S. Coulombe, H. Lee, A. K. Liljedahl, et al. Standardized monitoring of permafrost thaw: a user-friendly, multiparameter protocol. *Arctic Science*, 8(1):153–182, 2021.

J. Boike, S. M. Stuenzi, J. Gottuk, N. Bornemann, and B. Groenke. Arctic land expeditions in permafrost research. the moment project: Expedition to the arctic station, qeqertarsuaq, disko island and ilulissat, west greenland in 2022. *Berichte zur Polar-und Meeresforschung / Reports on polar and marine research*, 782:1–18, 2024.

C. Bonfils, T. Phillips, D. Lawrence, P. Cameron-Smith, W. Riley, and Z. Subin. On the influence of shrub height and expansion on northern high latitude climate. *Environmental Research Letters*, 7(1):015503, 2012.

T. V. Callaghan, T. R. Christensen, and E. J. Jantze. Plant and vegetation dynamics on disko island, west greenland: Snapshots separated by over 40 years. *Ambio*, 40:624–637, 2011.

F. S. Chapin III, M. S. Bret-Harte, S. E. Hobbie, and H. Zhong. Plant functional types as predictors of transient responses of arctic vegetation to global change. *Journal of vegetation Science*, 7(3):347–358, 1996.

F. S. Chapin III, M. Sturm, M. C. Serreze, J. P. McFadden, J. Key, A. H. Lloyd, A. McGuire, T. S. Rupp, A. H. Lynch, J. P. Schimel, et al. Role of land-surface changes in arctic summer warming. *science*, 310(5748):657–660, 2005.

W. Chen, K. D. Tape, E. S. Euskirchen, S. Liang, A. Matos, J. Greenberg, and J. M. Fraterrigo. Impacts of arctic shrubs on root traits and belowground nutrient cycles across a northern alaskan climate gradient. *Frontiers in Plant Science*, 11:588098, 2020.

S. R. Curasi, M. M. Loranty, and S. M. Natali. Water track distribution and effects on carbon dioxide flux in an eastern siberian upland tundra landscape. *Environmental Research Letters*, 11(4):045002, 2016.

E. Daly and A. Porporato. A review of soil moisture dynamics: from rainfall infiltration to ecosystem response. *Environmental engineering science*, 22(1):9–24, 2005.

L. D'Imperio, C. S. Nielsen, A. Westergaard-Nielsen, A. Michelsen, and B. Elberling. Methane oxidation in contrasting soil types: responses to experimental warming with implication for landscape-integrated ch4 budget. *Global Change Biology*, 23(2):966–976, 2017.

F. Domine, M. Barrere, and S. Morin. The growth of shrubs on high arctic tundra at bylot island: impact on snow physical properties and permafrost thermal regime. *Biogeosciences*, 13(23):6471–6486, 2016.

F. Domine, M. Belke-Brea, D. Sarrazin, L. Arnaud, M. Barrere, and M. Poirier. Soil moisture, wind speed and depth hoar formation in the arctic snowpack. *Journal of Glaciology*, 64 (248):990–1002, 2018.

A. Donateo, D. Famulari, D. Giovannelli, A. Mariani, M. Mazzola, S. Decesari, and G. Pappaccogli. Observations of methane net sinks in the arctic tundra. *EGUsphere*, 2024: 1–31, 2024.

S. C. Elmendorf, G. H. Henry, R. D. Hollister, R. G. Björk, N. Boulanger-Lapointe, E. J. Cooper, J. H. Cornelissen, T. A. Day, E. Dorrepaal, T. G. Elumeeva, et al. Plot-scale evidence of tundra vegetation change and links to recent summer warming. *Nature climate change*, 2(6):453–457, 2012.

S. C. Elmendorf, G. H. Henry, R. D. Hollister, A. M. Fosaa, W. A. Gould, L. Hermanutz, A. Hofgaard, I. S. Jónsdóttir, J. C. Jorgenson, E. Lévesque, et al. Experiment, monitoring, and gradient methods used to infer climate change effects on plant communities yield consistent patterns. *Proceedings of the National Academy of Sciences*, 112(2):448–452, 2015.

H. E. Epstein, M. K. Raynolds, D. A. Walker, U. S. Bhatt, C. J. Tucker, and J. E. Pinzon. Dynamics of aboveground phytomass of the circumpolar arctic tundra during the past three decades. *Environmental Research Letters*, 7(1):015506, 2012.

W. Eugster, W. R. Rouse, R. A. Pielke Sr, J. P. Mcfadden, D. D. Baldocchi, T. G. F. Kittel, F. S. Chapin III, G. E. Liston, P. L. Vidale, E. Vaganov, et al. Land–atmosphere energy exchange in arctic tundra and boreal forest: available data and feedbacks to climate. *Global change biology*, 6(S1):84–115, 2000.

G. V. Frost, H. E. Epstein, D. A. Walker, G. Matyshak, and K. Ermokhina. Seasonal and long-term changes to active-layer temperatures after tall shrubland expansion and succession in arctic tundra. *Ecosystems*, 21:507–520, 2018.

M. García Criado, I. H. Myers-Smith, A. D. Bjorkman, C. E. Lehmann, and N. Stevens. Woody plant encroachment intensifies under climate change across tundra and savanna biomes. *Global Ecology and Biogeography*, 29(5):925–943, 2020.

K. J. Gonzalez Martinez, D. Zona, T. Biggs, K. Bernabe, D. Sirivat, F. Tenorio, and W. Oechel. Environmental and vegetation control on active layer and soil temperature in an arctic tundra ecosystem in alaska. *Biogeosciences Discussions*, 2023:1–31, 2023.

J. Gornall, I. Jónsdóttir, S. Woodin, and R. Van der Wal. Arctic mosses govern below-ground environment and ecosystem processes. *Oecologia*, 153:931–941, 2007.

GRASS Development Team. *Geographic Resources Analysis Support System (GRASS*

GIS). Open Source Geospatial Foundation, 2022. URL https://grass.osgeo.org. Version 7.8.

Greenland Ecosystem Monitoring. GeoBasis Disko - Meteorology - AWS1-Meteorology (Version 1.0), 2024a. URL https://doi.org/10.17897/A22W-9Z72. Data set [CC-BY-SA-4.0].

Greenland Ecosystem Monitoring. GeoBasis Disko - Meteorology - AWS3-Meteorology (Version 1.0), 2024b. URL https://doi.org/10.17897/FEGK-0632. Data set [CC-BY-SA-4.0].

M. Grimes, J. L. Carrivick, M. W. Smith, and A. J. Comber. Land cover changes across greenland dominated by a doubling of vegetation in three decades. *Scientific Reports*, 14(1):3120, 2024.

I. Grünberg, E. J. Wilcox, S. Zwieback, P. Marsh, and J. Boike. Linking tundra vegetation, snow, soil temperature, and permafrost. *Biogeosciences*, 17(16):4261–4279, 2020.

K. C. Guay, P. S. Beck, L. T. Berner, S. J. Goetz, A. Baccini, and W. Buermann. Vegetation productivity patterns at high northern latitudes: A multi-sensor satellite data assessment. *Global change biology*, 20(10):3147–3158, 2014.

B. U. Hansen, B. Elberling, O. Humlum, and N. Nielsen. Meteorological trends (1991–2004) at arctic station, central west greenland (69 15'n) in a 130 years perspective. *Geografisk Tidsskrift-Danish Journal of Geography*, 106(1):45–55, 2006.

M. M. Heijmans, R. Í. Magnússon, M. J. Lara, G. V. Frost, I. H. Myers-Smith, J. van Huissteden, M. T. Jorgenson, A. N. Fedorov, H. E. Epstein, D. M. Lawrence, et al. Tundra vegetation change and impacts on permafrost. *Nature Reviews Earth & Environment*, 3 (1):68–84, 2022.

L. Hinzman, D. Kane, R. Gieck, and K. Everett. Hydrologic and thermal properties of the active layer in the alaskan arctic. *Cold Regions Science and Technology*, 19(2):95–110, 1991.

J. Hollesen, A. Buchwal, G. Rachlewicz, B. U. Hansen, M. O. Hansen, O. Stecher, and B. Elberling. Winter warming as an important co-driver for betula nana growth in western greenland during the past century. *Global Change Biology*, 21(6):2410–2423, 2015.

J. L. Horton and S. C. Hart. Hydraulic lift: a potentially important ecosystem process. *Trends in ecology & evolution*, 13(6):232–235, 1998.

C. Jackisch, K. Germer, T. Graeff, I. Andrä, K. Schulz, M. Schiedung, J. Haller-Jans, J. Schneider, J. Jaquemotte, P. Helmer, et al. Soil moisture and matric potential–an open field comparison of sensor systems. *Earth System Science Data*, 12(1):683–697, 2020.

F. Jaroszynska, I. Althuizen, A. H. Halbritter, K. Klanderud, H. Lee, R. J. Telford, and V. Vandvik. Bryophytes dominate plant regulation of soil microclimate in alpine grasslands. *Oikos*, page e10091, 2023.

I. Juszak, W. Eugster, M. M. Heijmans, and G. Schaepman-Strub. Contrasting radiation and soil heat fluxes in arctic shrub and wet sedge tundra. *Biogeosciences*, 13(13):4049–4064, 2016.

J. Kemppinen, P. Niittynen, A. Virkkala, K. Happonen, H. Riihimaki, J. Aalto, and M. Luoto. Dwarf shrubs impact tundra soils: Drier, colder, and less organic carbon. *Ecosystems*, 2021.

J. Kemppinen, P. Niittynen, T. Rissanen, V. Tyystjärvi, J. Aalto, and M. Luoto. Soil moisture variations from boreal forests to the tundra. *Water Resources Research*, 59(6): e2022WR032719, 2023.

M. Kopeckỳ, M. Macek, and J. Wild. Topographic wetness index calculation guidelines based on measured soil moisture and plant species composition. *Science of the Total Environment*, 757:143785, 2021.

D. M. Lawrence, C. D. Koven, S. C. Swenson, W. J. Riley, and A. Slater. Permafrost thaw and resulting soil moisture changes regulate projected high-latitude co2 and ch4 emissions. *Environmental Research Letters*, 10(9):094011, 2015.

D. R. Legates, R. Mahmood, D. F. Levia, T. L. DeLiberty, S. M. Quiring, C. Houser, and F. E. Nelson. Soil moisture: A central and unifying theme in physical geography. *Progress in Physical Geography*, 35(1):65–86, 2011.

M. Litaor, M. Williams, and T. Seastedt. Topographic controls on snow distribution, soil moisture, and species diversity of herbaceous alpine vegetation, niwot ridge, colorado. *Journal of Geophysical Research: Biogeosciences*, 113(G2), 2008.

M. M. Loranty, B. W. Abbott, D. Blok, T. A. Douglas, H. E. Epstein, B. C. Forbes, B. M. Jones, A. L. Kholodov, H. Kropp, A. Malhotra, et al. Reviews and syntheses: Changing ecosystem influences on soil thermal regimes in northern high-latitude permafrost regions. *Biogeosciences*, 15(17):5287–5313, 2018.

M. Mallen-Cooper, B. J. Graae, and W. K. Cornwell. Lichens buffer tundra microclimate more than the expanding shrub betula nana. *Annals of Botany*, 128(4):407–418, 2021.

M. Man, V. Kalcík, M. Macek, J. Bruna, L. Hederová, J. Wild, and M. Kopecký. myclim: Microclimate data handling and standardised analyses in r. *Methods in Ecology and Evolution*, 14(9):2308–2320, 2023.

P. Miller, P. Webber, W. Oechel, and L. Tieszen. Biophysical processes and primary production. *An Arctic ecosystem: the coastal tundra at Barrow, Alaska*, pages 66–101, 1980.

I. H. Myers-Smith and D. S. Hik. Shrub canopies influence soil temperatures but not nutrient dynamics: an experimental test of tundra snow–shrub interactions. *Ecology and evolution*, 3(11):3683–3700, 2013.

S. M. Natali, E. A. Schuur, M. Mauritz, J. D. Schade, G. Celis, K. G. Crummer, C. Johnston, J. Krapek, E. Pegoraro, V. G. Salmon, et al. Permafrost thaw and soil moisture driving co2 and ch4 release from upland tundra. *Journal of Geophysical Research: Biogeosciences*, 120(3):525–537, 2015.

J. Obu. How much of the earth's surface is underlain by permafrost? *Journal of Geophysical Research: Earth Surface*, 126(5):e2021JF006123, 2021.

J. A. O'Donnell, V. E. Romanovsky, J. W. Harden, and A. D. McGuire. The effect of moisture content on the thermal conductivity of moss and organic soil horizons from black spruce ecosystems in interior alaska. *Soil Science*, 174(12):646–651, 2009.

J. Oehri, G. Schaepman-Strub, J.-S. Kim, R. Grysko, H. Kropp, I. Grünberg, V. Zemlianskii, O. Sonnentag, E. S. Euskirchen, M. Reji Chacko, et al. Vegetation type is an important

predictor of the arctic summer land surface energy budget. *Nature communications*, 13 (1):6379, 2022.

D. Olefeldt, M. R. Turetsky, P. M. Crill, and A. D. McGuire. Environmental and physical controls on northern terrestrial methane emissions across permafrost zones. *Global change biology*, 19(2):589–603, 2013.

R. G. Pearson, S. J. Phillips, M. M. Loranty, P. S. Beck, T. Damoulas, S. J. Knight, and S. J. Goetz. Shifts in arctic vegetation and associated feedbacks under climate change. *Nature climate change*, 3(7):673–677, 2013.

D. Penna, M. Borga, D. Norbiato, and G. Dalla Fontana. Hillslope scale soil moisture variability in a steep alpine terrain. *Journal of Hydrology*, 364(3-4):311–327, 2009.

S. Petters, M. Varsadiya, P. Liebmann, J. Schnecker, G. Guggenberger, J. Bárta, and T. Urich. Census of below-ground biota associated with permafrost affected soils of western greenland, with a focus on trophic structure. *European Journal of Soil Biology*, 121: 103623, 2024.

QGIS Development Team. *QGIS Geographic Information System*. Open Source Geospatial Foundation Project, 2019. URL `https://qgis.org`. Version 3.6.

R Core Team. *R: A Language and Environment for Statistical Computing*. R Foundation for Statistical Computing, Vienna, Austria, 2021. URL `https://www.R-project.org/`.

M. K. Raynolds, D. A. Walker, A. Balser, C. Bay, M. Campbell, M. M. Cherosov, F. J. Daniëls, P. B. Eidesen, K. A. Ermokhina, G. V. Frost, et al. A raster version of the circumpolar arctic vegetation map (cavm). *Remote Sensing of Environment*, 232:111297, 2019.

N. Rößger, T. Sachs, C. Wille, J. Boike, and L. Kutzbach. Seasonal increase of methane emissions linked to warming in siberian tundra. *Nature Climate Change*, 12(11):1031–1036, 2022.

D. Scherrer and C. Körner. Topographically controlled thermal-habitat differentiation buffers alpine plant diversity against climate warming. *Journal of biogeography*, 38(2):406–416, 2011.

P. Scholl, D. Leitner, G. Kammerer, W. Loiskandl, H.-P. Kaul, and G. Bodner. Root induced changes of effective 1d hydraulic properties in a soil column. *Plant and soil*, 381:193–213, 2014.

E. A. Schuur, A. D. McGuire, C. Schädel, G. Grosse, J. W. Harden, D. J. Hayes, G. Hugelius, C. D. Koven, P. Kuhry, D. M. Lawrence, et al. Climate change and the permafrost carbon feedback. *Nature*, 520(7546):171–179, 2015.

S. Schuuring, R. Halvorsen, P. Bronken Eidesen, P. Niittynen, J. Kemppinen, and S. I. Lang. High arctic vegetation communities with a thick moss layer slow active layer thaw. *Journal of Geophysical Research: Biogeosciences*, 129(8):e2023JG007880, 2024.

N. I. Shiklomanov, D. A. Streletskiy, F. E. Nelson, R. D. Hollister, V. E. Romanovsky, C. E. Tweedie, J. G. Bockheim, and J. Brown. Decadal variations of active-layer thickness in moisture-controlled landscapes, barrow, alaska. *Journal of Geophysical Research: Biogeosciences*, 115(G4), 2010.

N. A. Soudzilovskaia, P. M. van Bodegom, and J. H. Cornelissen. Dominant bryophyte control over high-latitude soil temperature fluctuations predicted by heat transfer traits, field moisture regime and laws of thermal insulation. *Functional Ecology*, 27(6):1442–1454, 2013.

T. F. Stepinski and J. Jasiewicz. Geomorphons-a new approach to classification of landforms. *Proceedings of geomorphometry*, 2011:109–112, 2011.

P. C. Stoy, L. E. Street, A. V. Johnson, A. Prieto-Blanco, and S. A. Ewing. Temperature, heat flux, and reflectance of common subarctic mosses and lichens under field conditions: might changes to community composition impact climate-relevant surface fluxes? *Arctic, antarctic, and alpine research*, 44(4):500–508, 2012.

M. Sturm, J. Holmgren, J. P. McFadden, G. E. Liston, F. S. Chapin, and C. H. Racine. Snow–shrub interactions in arctic tundra: a hypothesis with climatic implications. *Journal of Climate*, 14(3):336–344, 2001.

M. Sturm, J. Schimel, G. Michaelson, J. M. Welker, S. F. Oberbauer, G. E. Liston, J. Fahnestock, and V. E. Romanovsky. Winter biological processes could help convert arctic tundra to shrubland. *Bioscience*, 55(1):17–26, 2005.

B. N. Sulman, V. G. Salmon, C. M. Iversen, A. L. Breen, F. Yuan, and P. E. Thornton. Integrating arctic plant functional types in a land surface model using above-and belowground field observations. *Journal of Advances in Modeling Earth Systems*, 13(4): e2020MS002396, 2021.

S. A. Sundstøl and A. Odland. Responses of alpine vascular plants and lichens to soil temperatures. In *Annales Botanici Fennici*, volume 54, pages 17–28. BioOne, 2017.

K. Tape, M. Sturm, and C. Racine. The evidence for shrub expansion in northern alaska and the pan-arctic. *Global change biology*, 12(4):686–702, 2006.

C. Tarnocai, J. G. Canadell, E. A. Schuur, P. Kuhry, G. Mazhitova, and S. Zimov. Soil organic carbon pools in the northern circumpolar permafrost region. *Global biogeochemical cycles*, 23(2), 2009.

H.-J. van der Kolk, M. M. Heijmans, J. Van Huissteden, J. W. Pullens, and F. Berendse. Potential arctic tundra vegetation shifts in response to changing temperature, precipitation and permafrost thaw. *Biogeosciences*, 13(22):6229–6245, 2016.

R. Van der Wal and R. Brooker. Mosses mediate grazer impacts on grass abundance in arctic ecosystems. *Functional Ecology*, 18(1):77–86, 2004.

A.-M. Virkkala, P. Niittynen, J. Kemppinen, M. E. Marushchak, C. Voigt, G. Hensgens, J. Kerttula, K. Happonen, V. Tyystjärvi, C. Biasi, et al. High-resolution spatial patterns and drivers of terrestrial ecosystem carbon dioxide, methane, and nitrous oxide fluxes in the tundra. *Biogeosciences Discussions*, 2023:1–29, 2023.

J. Von Oppen, J. J. Assmann, A. D. Bjorkman, U. A. Treier, B. Elberling, J. Nabe-Nielsen, and S. Normand. Cross-scale regulation of seasonal microclimate by vegetation and snow in the arctic tundra. *Global Change Biology*, 28(24):7296–7312, 2022.

D. A. Walker, M. K. Raynolds, F. J. Daniëls, E. Einarsson, A. Elvebakk, W. A. Gould, A. E. Katenin, S. S. Kholod, C. J. Markon, E. S. Melnikov, et al. The circumpolar arctic vegetation map. *Journal of vegetation science*, 16(3):267–282, 2005.

J. A. Wiens. Spatial scaling in ecology. *Functional ecology*, 3(4):385–397, 1989.

J. Wild, M. Kopeckỳ, M. Macek, M. Šanda, J. Jankovec, and T. Haase. Climate at ecologically relevant scales: A new temperature and soil moisture logger for long-term microclimate measurement. *Agricultural and Forest Meteorology*, 268:40–47, 2019.

W. Xu, A. Prieme, E. J. Cooper, M. A. Mörsdorf, P. Semenchuk, B. Elberling, P. Grogan, and P. L. Ambus. Deepened snow enhances gross nitrogen cycling among pan-arctic tundra soils during both winter and summer. *Soil Biology and Biochemistry*, 160:108356, 2021.

T. Zhang. Influence of the seasonal snow cover on the ground thermal regime: An overview. *Reviews of Geophysics*, 43(4), 2005.

W. Zhang, P.-E. Jansson, C. Sigsgaard, A. McConnell, M. M. Jammet, A. Westergaard-Nielsen, M. Lund, T. Friborg, A. Michelsen, and B. Elberling. Model-data fusion to assess year-round co2 fluxes for an arctic heath ecosystem in west greenland (69 n). *Agricultural and Forest Meteorology*, 272:176–186, 2019.

D. Zona, P. M. Lafleur, K. Hufkens, B. Gioli, B. Bailey, G. Burba, E. S. Euskirchen, J. D. Watts, K. A. Arndt, M. Farina, et al. Pan-arctic soil moisture control on tundra carbon sequestration and plant productivity. *Global Change Biology*, 29(5):1267–1281, 2023.

S. Zwieback, Q. Chang, P. Marsh, and A. Berg. Shrub tundra ecohydrology: rainfall interception is a major component of the water balance. *Environmental Research Letters*, 14 (5):055005, 2019.

A APPENDIX

A.1 Temperature and Moisture Data

Table 2: Coordinates of the temperature-moisture sensors located in Blæsedalen in the South of Qeqertarsuaq (Disko Island), Western Greenland. Latitude and longitude given in WGS84 coordinate reference system (EPSG:4326) for each plot by transect and vegetation unit.

Transect 1				Transect 3			
Veg. Unit	**Plot ID**	**Lat**	**Lon**	**Veg. Unit**	**Plot ID**	**Lat**	**Lon**
E	16	69.2677	-53.4669	A	1	69.2787	-53.4794
E	17	69.2676	-53.4668	A	5	69.2786	-53.4796
E	18	69.2678	-53.4670	A	6	69.2789	-53.4794
F	19	69.2680	-53.4661	B	7	69.2787	-53.4777
F	20	69.2678	-53.4662	B	8	69.2787	-53.4775
F	21	69.2679	-53.4665	B	9	69.2788	-53.4778
G	22	69.2681	-53.4653	C	10	69.2786	-53.4748
G	23	69.2681	-53.4650	C	11	69.2788	-53.4757
G	24	69.2681	-53.4652	C	12	69.2790	-53.4757
H	25	69.2687	-53.4625	D	13	69.2788	-53.4742
H	26	69.2687	-53.4624	D	14	69.2787	-53.4743
H	27	69.2688	-53.4626	D	15	69.2787	-53.4741

A.1.1 Moisture Data: Raw Signal Conversion

The formula for raw moisture signal conversion of unknown soils provided by Kopeckỳ et al. (2021) (from supplementary material):

$$\text{Volumetric Water Content} = -1.34 \times 10^{-8}x^2 + 2.50 \times 10^{-4}x - 0.16 \quad (1)$$

To come up with the equation, the authors combined measurements of six soil samples classified as loam, silt loam, sandy loam and loamy sand before modeling the calibration curve (Fig. 16). The curve lies approximately at the position of the 'sandy loam A' curve established by Wild et al. (2019), visible in 17. Only the calibration curve for peat soils and 'loamy sand B' are even steeper and lie above the universal conversion curve. To conclude: for soil moisture values converted with the universal formula, moisture is potentially underestimated in organic soils (peat) and potentially overestimated for other soil types, especially those classified as sand and silt loam.

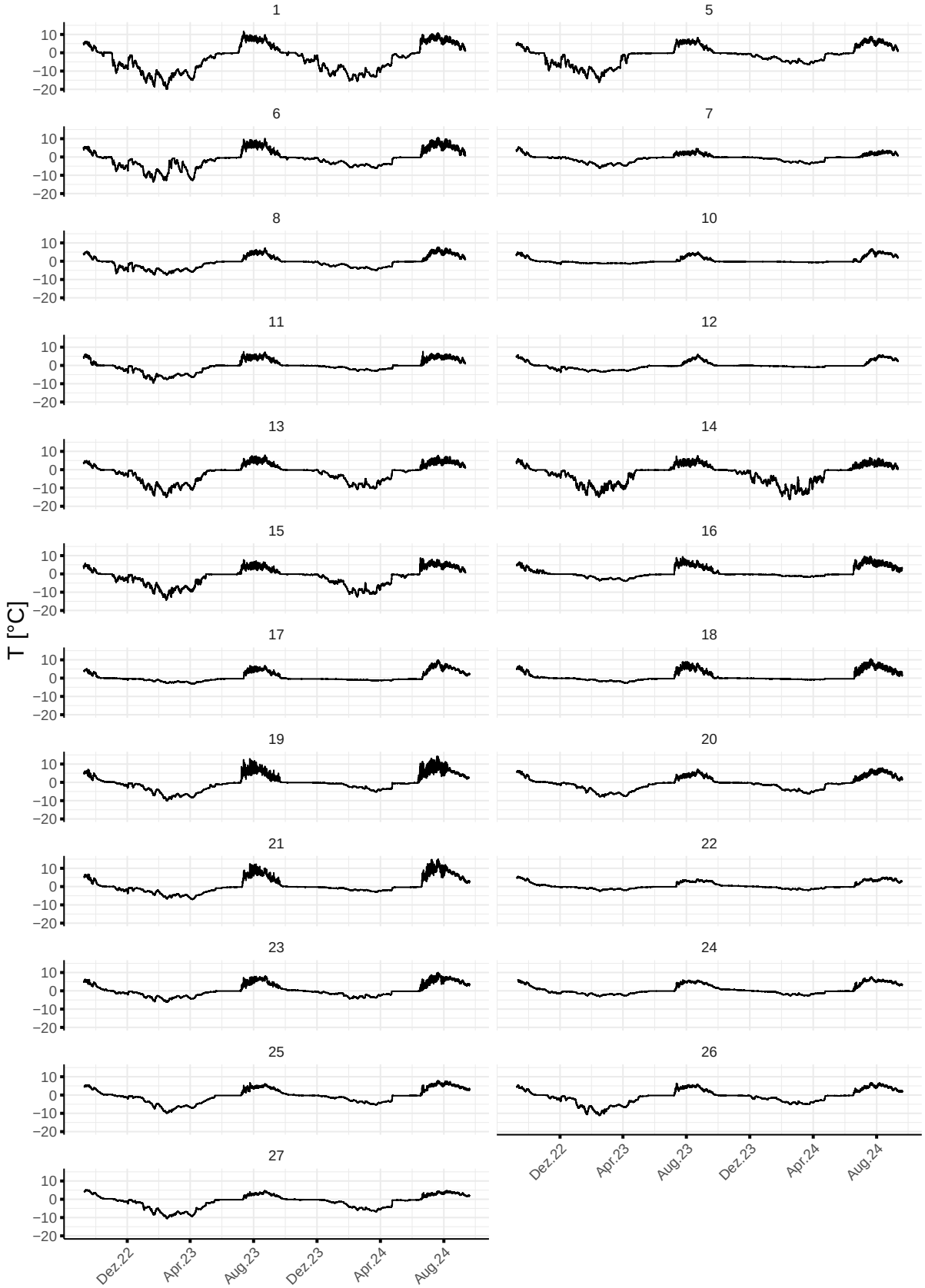

Figure 15: Complete soil temperature time series for each temperature-moisture sensor after cleaning the data and applying the ice-bath calibration.

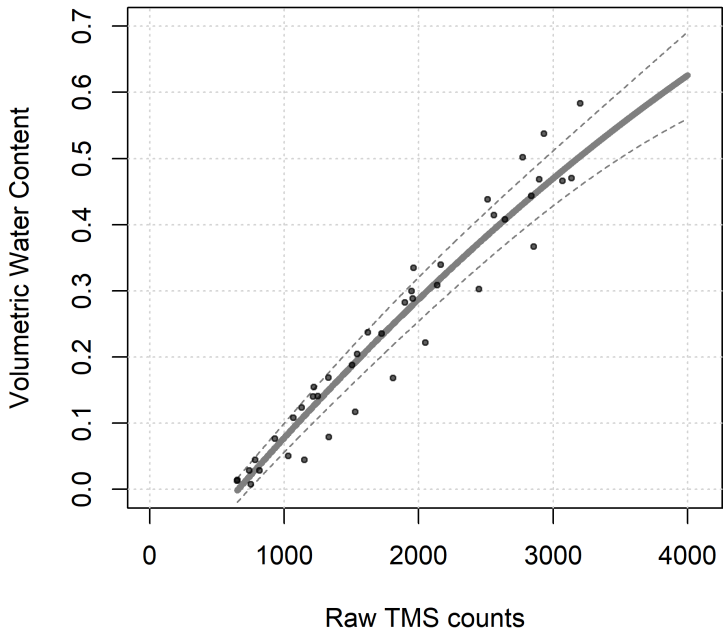

Figure 16: Calibration curve for conversion of raw soil moisture measurements recorded by TOMST TMS-4 temperature-moisture sensors using time-domanin reflectometry (here: "Raw TMS counts") to soil moisture given as volumetric water content (here: "volumetric water content"). The formula is derived from laboratory measurements performed by Kopeckỳ et al. (2021). The solid line shows the fit and dashed lines 95% confidence interval from the mixed-effect model they used for their approach.

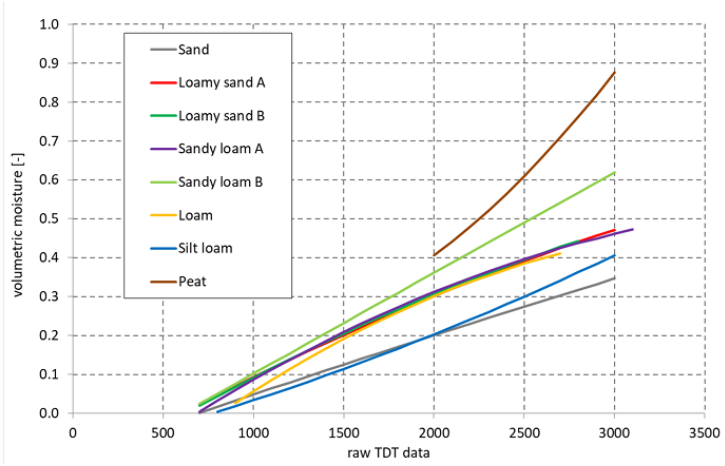

Figure 17: Calibration curves derived from laboratory measurements performed by Wild et al. (2019) to convert raw soil moisture measurements recorded by TOMST TMS-4 temperature-moisture sensors using time-domanin reflectometry (here: "Raw TDT data") to soil moisture given as volumetric water content (here "volumetric moisture") for different soil types (see Wild et al. (2019) for detailed description of the classes).

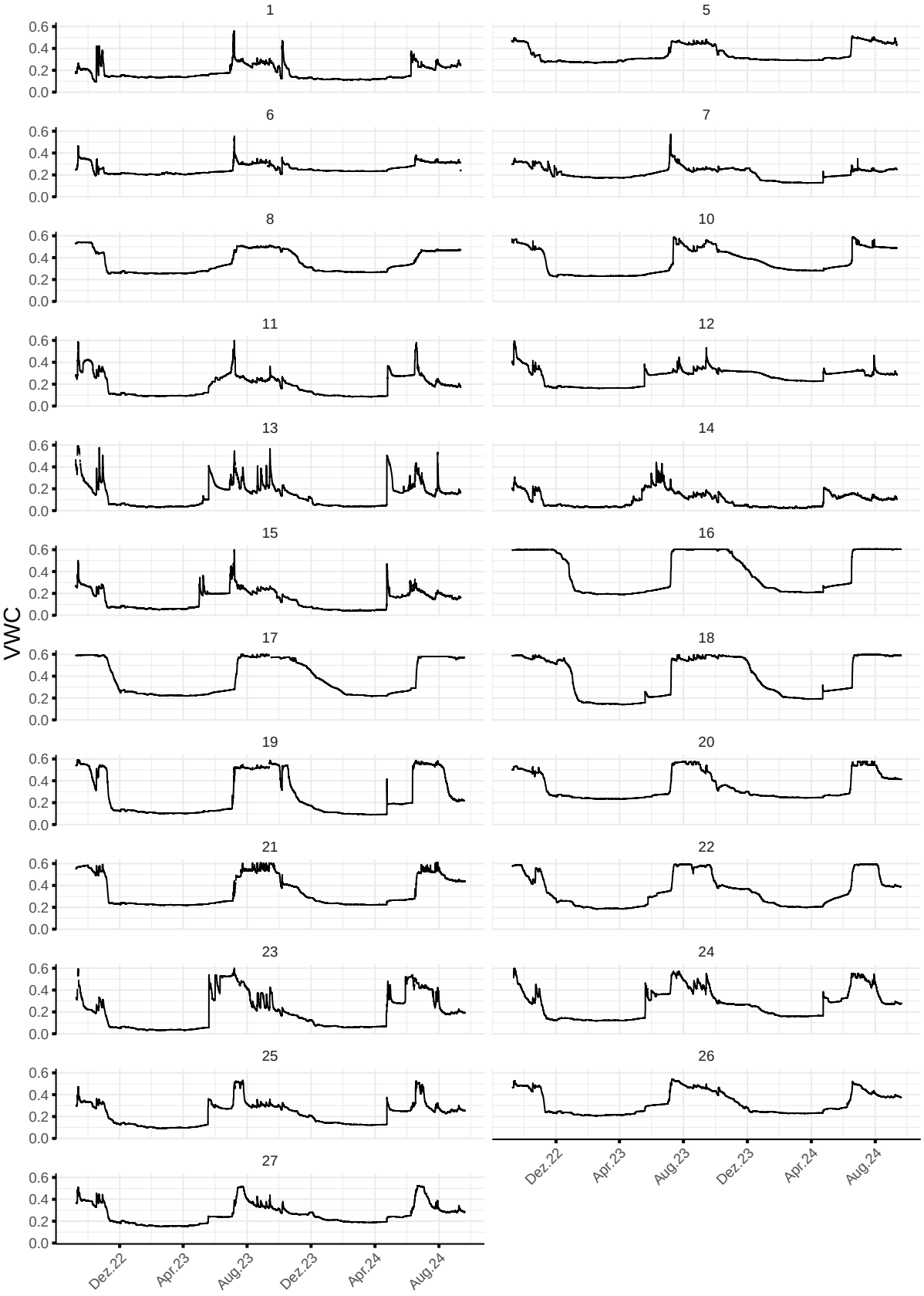

Figure 18: Complete soil moisture time series for each temperature-moisture sensor after cleaning the data and converting it from raw electromagnetic pulses to soil moisture given as volumetric water content (VWC) of the upper soil (0 - 15 cm) using a formula provided by Kopeckỳ et al. (2021).

A.1.2 Moisture Data: Verification

Table 3: Coordinates of the soil samples locations located in Blæsedalen in the South of Qeqertarsuaq (Disko Island), Western Greenland. Latitude and longitude given in WGS84 coordinate reference system (EPSG: 4326). Named after closest temperature-moisture sensor with respective distance to the sensor and depth at which the sample was taken.

Sample Name	Distance to sensor (m)	Latitude	Longitude	Profile Depth
$S1_I$	0.0	69.2787	-53.4794	2-7 cm
$S1_{II}$	0.0	69.2787	-53.4794	2-7 cm
$S7_I$	6.6	69.2788	-53.4779	12-17 cm
$S7_{II}$	6.6	69.2788	-53.4779	12-17 cm
$S10_I$	19.8	69.2787	-53.4751	12-17 cm
$S10_{II}$	19.8	69.2787	-53.4751	12-17 cm
$S13_I$	9.1	69.2780	-53.4745	19-24 cm
$S13_{II}$	9.1	69.2780	-53.4745	18-23 cm
$S20_I$	3.4	69.2678	-53.4662	5-10 cm
$S20_{II}$	3.4	69.2678	-53.4662	9-14 cm
$S25_I$	4.6	69.2688	-53.4626	7-12 cm
$S25_{II}$	4.6	69.2688	-53.4626	7-12 cm

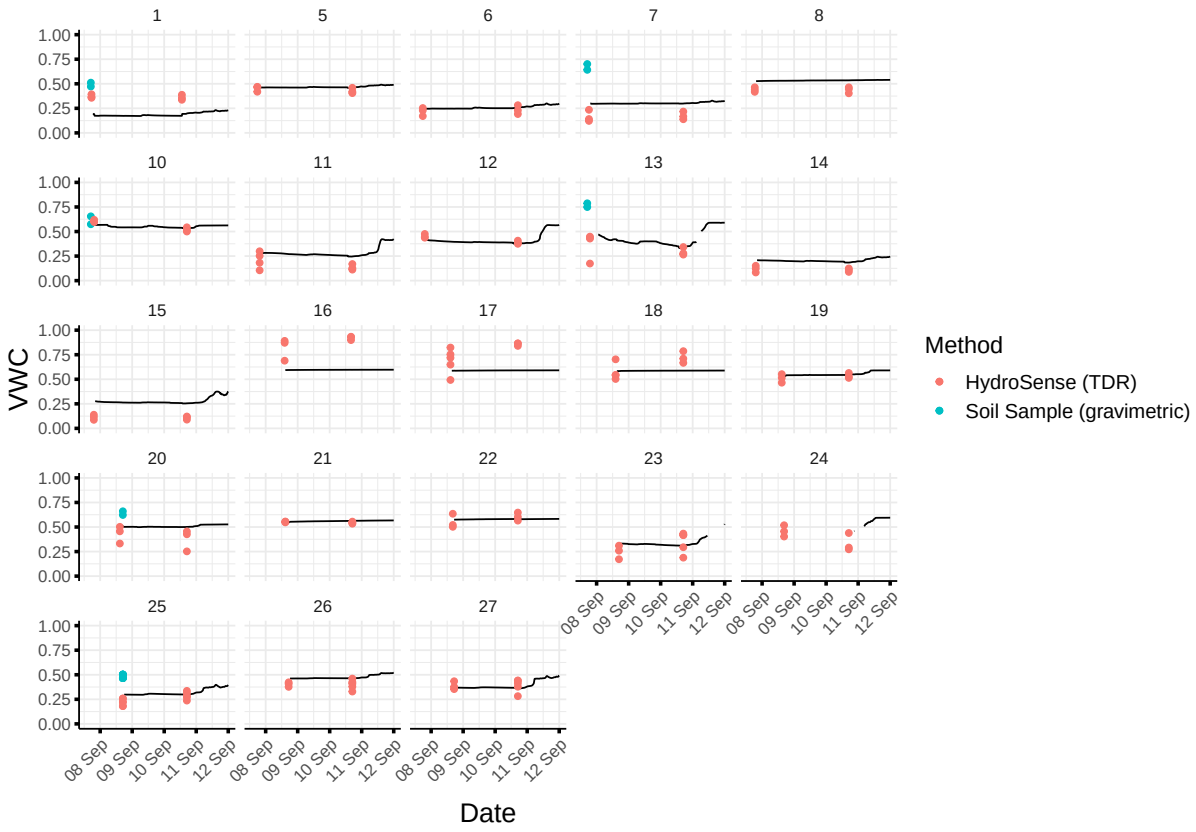

Figure 19: Adjusted TMS time series showing soil moisture given as volumetric water content (VWC) of the upper soil (0 - 15 cm) after installation of the TMS sensors with verification soil moisture measurements derived from soil samples (gravimetric) and a HydroSense II device based on time-domain reflectance (TDR). Point measurements either show true timing or, if only date was available, 17:00. For the comparison in Fig. 6, the point measurements were matched up with the TMS measurement closest in time.

A.2 Vegetation Data

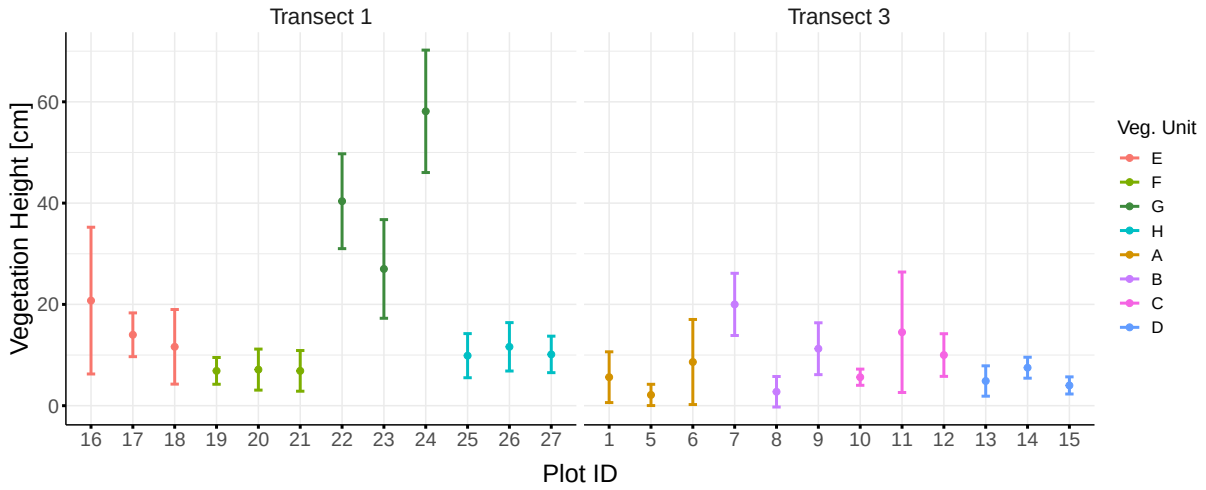

Figure 20: Mean vegetation height measured in September 2022 and September 2023 at 4 respective points within each plot in the study area with standard deviation. Colored by vegetation unit.

Table 4: Most common species recorded during field campaigns in September 2022 and September 2023 at the study site in Blæsedalen, Disko Island grouped by Plant Functional Type (PFT).

Plant Functional Type	Species
Forbs	Bistorta Vivipara
	Equisetum
	Farn
	Sabulina Rubella
	Other flowering plants
Graminoids	Eriophorum
	Sedges
Lichen	Lichen
Moss	Moss
Shrubs	Betula Nana
	Cassiope Tetragona
	Empetrum Nigrum
	Salix Glauca
	Vaccinium Uliginosum
	Vaccinium Vitis

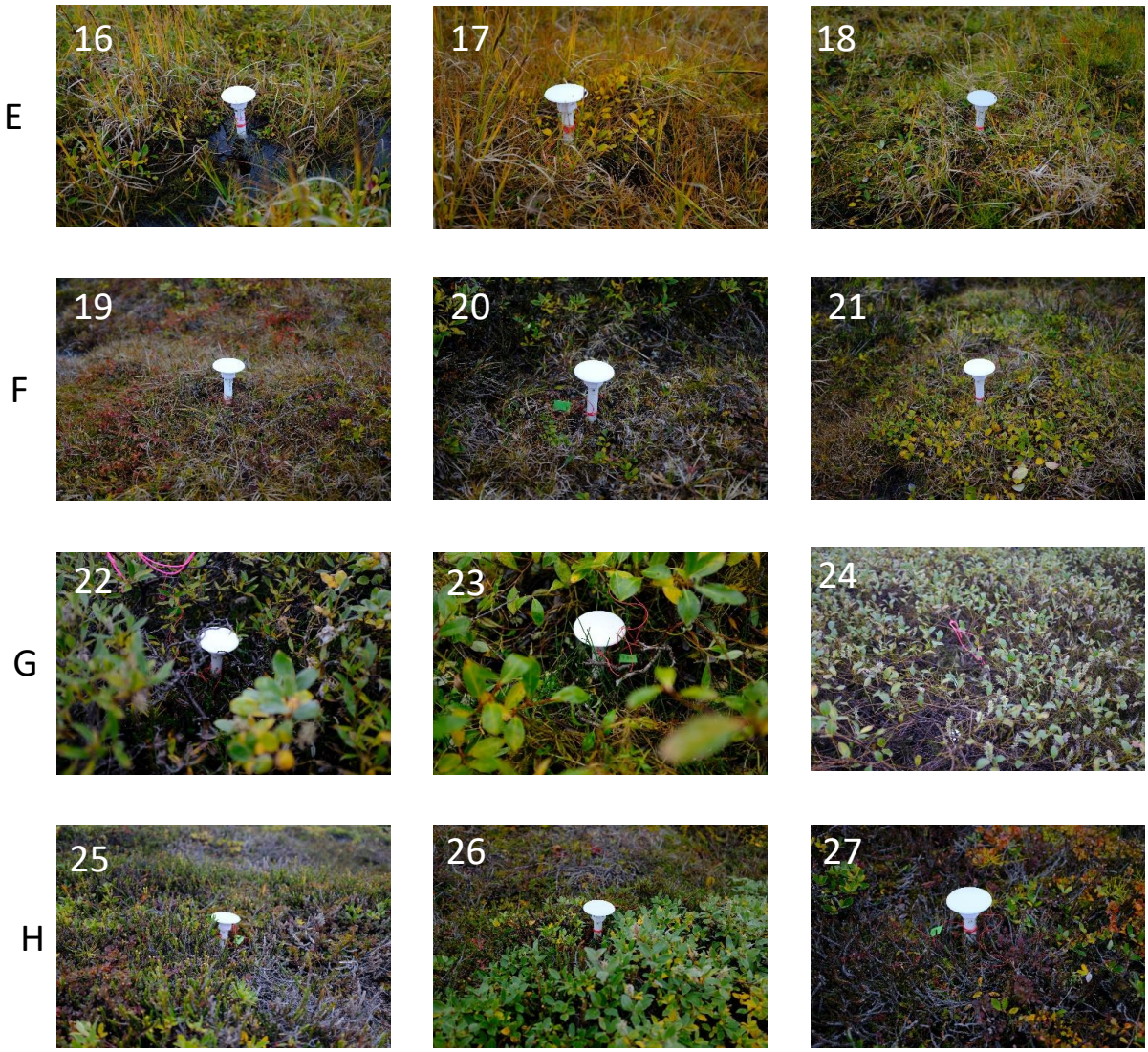

Figure 21: Plots located at transect 1 in Blæsedalen in the South of Qeqertarsuaq (Disko Island), Western Greenland. Images show vegetation and temperature-moisture sensors with plot ID. Each row represents one vegetation unit, starting from lowest to highest elevation. Taken by Julia Boike and Jannika Gottuk during 2022 field campaign (Boike et al., 2024).

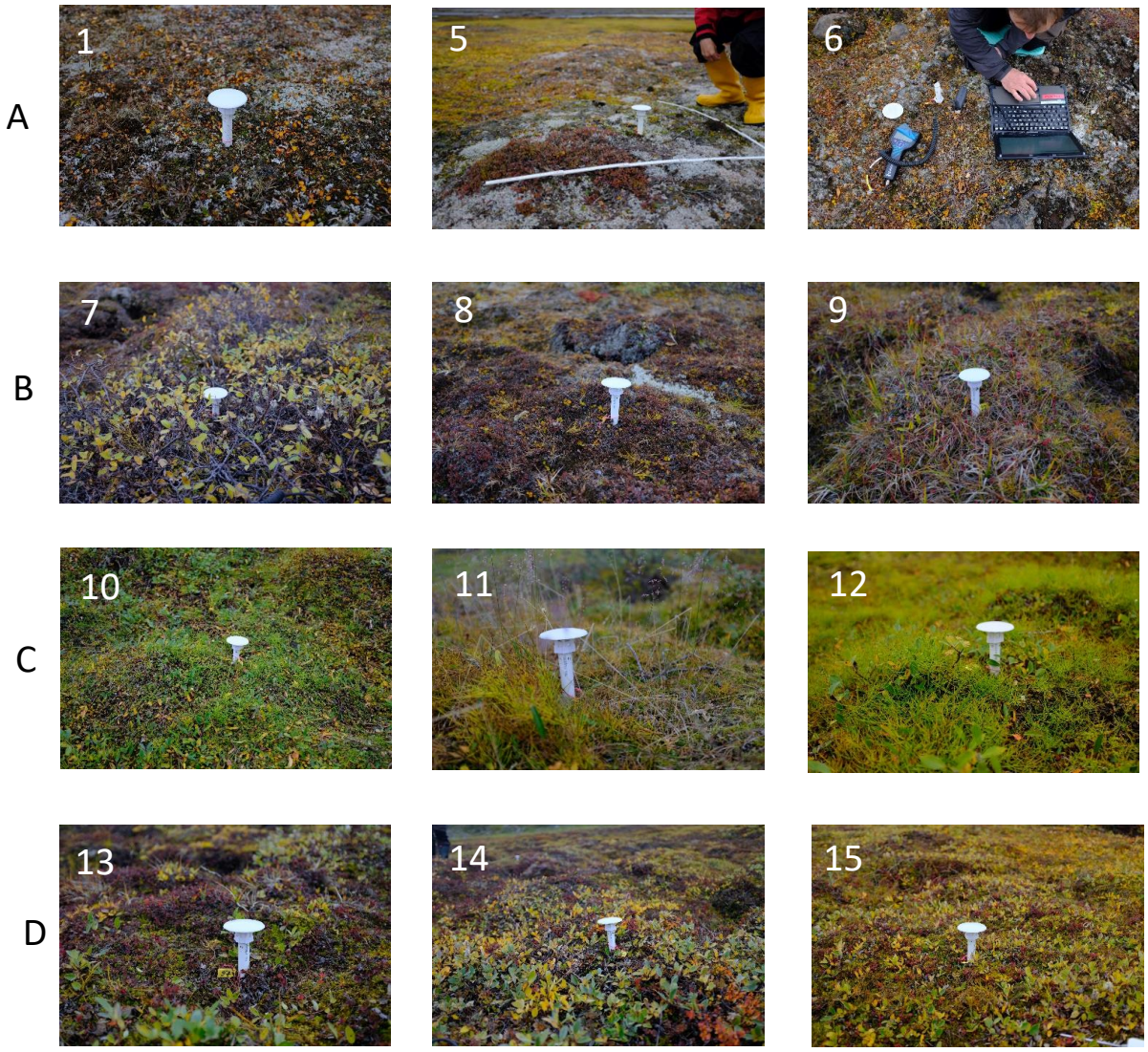

Figure 22: Plots located at transect 3 in Blæsedalen in the South of Qeqertarsuaq (Disko Island), Western Greenland. Images show vegetation and temperature-moisture sensors with plot ID. Each row represents one vegetation unit, starting from lowest to highest elevation. Taken by Julia Boike and Jannika Gottuk during 2022 field campaign (Boike et al., 2024).

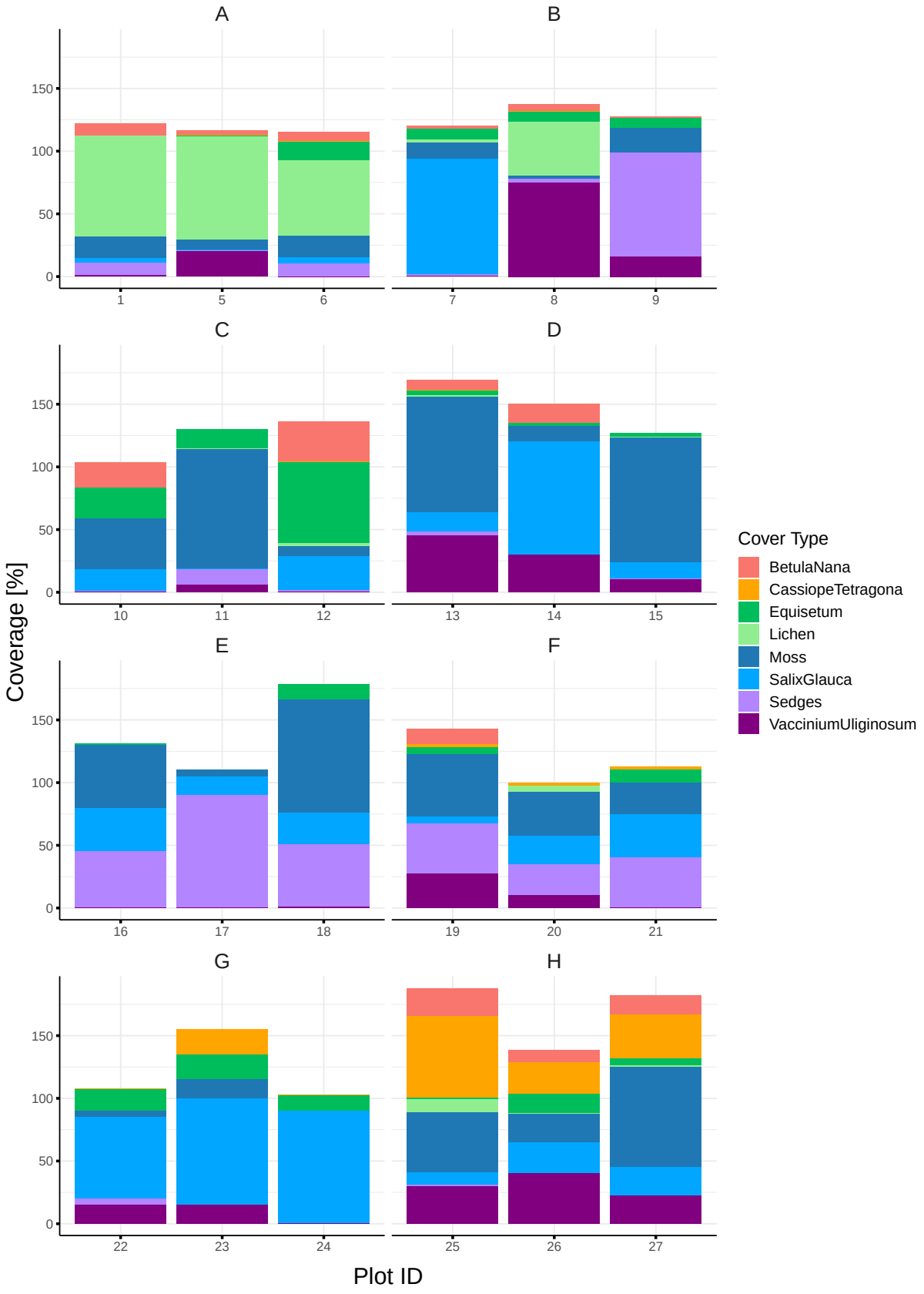

Figure 23: Vegetation composition for each plot in the study area by vegetation unit. Cover percentages are averaged over two observations from September 2022 and September 2023, all vegetation types shown have an accumulated minimum cover percentage of 50% in both respective years.

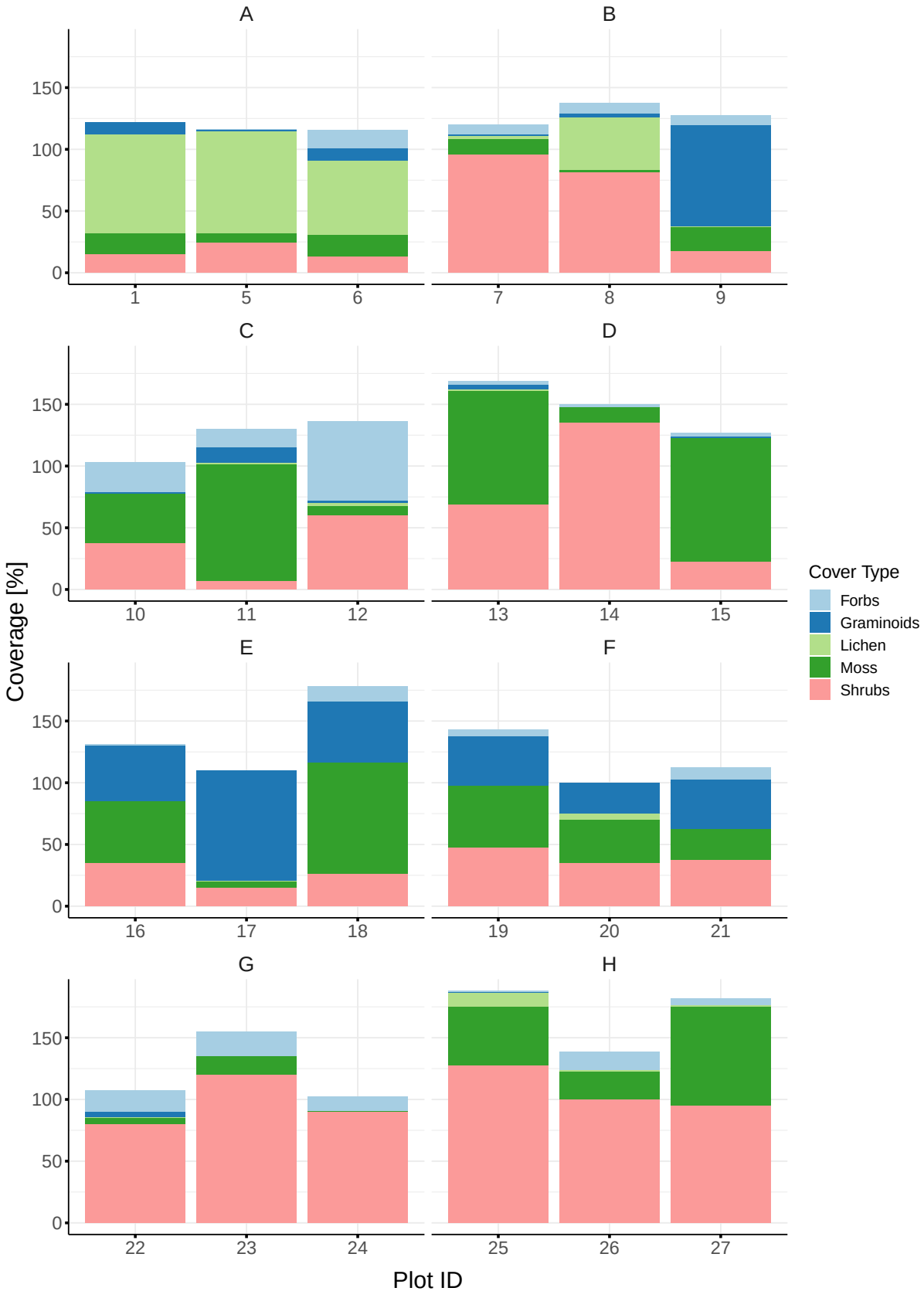

Figure 24: Vegetation composition after classification into plant functional types for each plot by vegetation unit. Cover percentages are averaged over two observations from September 2022 and September 2023.

A.3 Landform Classification: Geomorphons

Geomorphons describe common topographic landforms and they can be used to classify terrain features from a digital elevation model (DEM) at different scales at the same time. For my terrain classification I used the method proposed by Stepinski and Jasiewicz (2011) which is implemented as *r.geomorphons* in GRASSGIS (GRASS Development Team, 2022) and accessed via QGIS (QGIS Development Team, 2019).

This pattern recognition approach to terrain classification is based on neighborhood analysis, making use of computer vision techniques. Usually, in neighborhood analysis a local binary or local ternary pattern (LBP/LTP) is derived for a fixed neighborhood surrounding each pixel: Each neighboring cell is assigned a value based on its relative elevation to the center pixel (above/below: binary pattern, above/below/equal: ternary pattern). The resulting pattern is then matched to a corresponding landform type. However, topographical features are nested and the detected landform type depends on the neighborhood that is chosen. The approach by Stepinski and Jasiewicz (2011) uses the line-of-sight principle to classify each pixel within a self-adapting neighborhood, depending on the openness of the surrounding terrain. The user has the option of fine-tuning the algorithm using a number of parameters: The *search radius* sets the maximum distance for neighboring pixels. According to the authors, an infinite search radius should identify every feature at its appropriate scale, and the quest is to find the finite search radius at which computational effort is still reasonable but the classification converges (changes are minimal). The *skip distance* parameter allows the user to set a minimum distance from the center cell to start searching, thereby controlling the size of the resulting features. The *flatness* parameter is the maximum angle between the two lines at which the terrain is considered flat. Larger flatness angles lead to more flat areas. The *flatness distance* defines the radius within which the algorithm assesses terrain flatness with larger distances capturing broader landscape features and smaller distances focusing on more localized flat areas.

After systematically testing different combinations I chose the values in Tab. 5. I further simplified the result by merging some of the classes with similar neighbourhood configurations (summit and ridge, shoulder and spur, footslope and hollow, valley and depression) using the *Reclassify by table* tool in QGIS. Lastly, I created a mask for the lake by using the polygonize tool on the DEM in QGIS. The final classification is shown in Fig. Fig. 25.

Table 5: Final parameter setting for the geomorphons tool in QGIS (Stepinski and Jasiewicz, 2011) to classify the landscape into common feature types (geomorphons) based on a digital terrain model.

Search Radius	Skip Distance	Flatness	Flatness Distance
400 m	10 m	2°	0

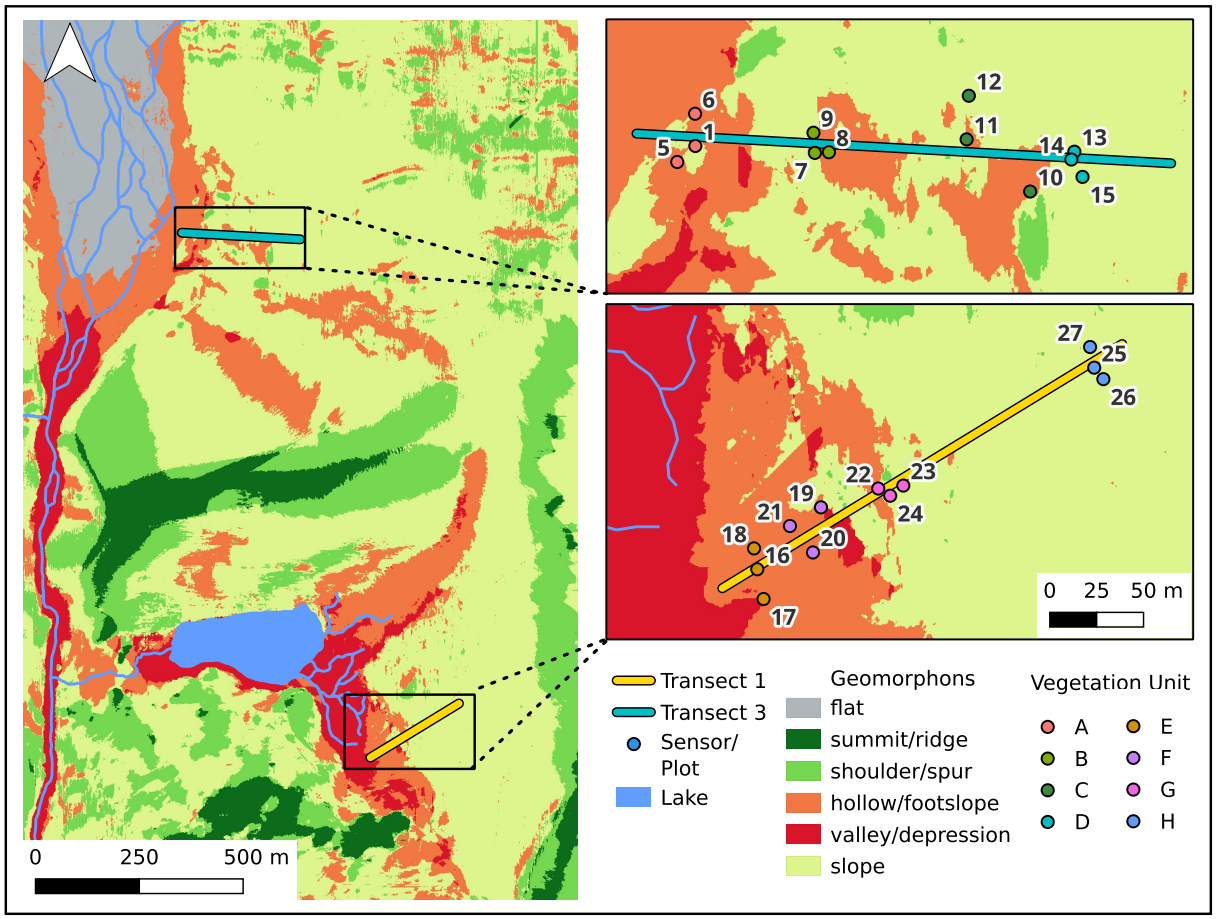

Figure 25: Topographical landform classification of the study region located in Blæsedalen in the South of Qeqertarsuaq (Disko Island), Western Greenland. The map was generated following the geomorphons approach proposed by Stepinski and Jasiewicz (2011) based on a digital terrain model provided by the Federal Agency for Cartography and Geodesy's Satellite-Based Crisis and Situation Service (*Bundesamt für Kartographie und Geodäsie, Satellitengestützter Krisen- und Lagedienst*). After applying the geomorphon algorithm implemented in QGIS, some classes were further summarized (e.g. hollow and footslope). *Left:* Overview showing transects 1 and 3 with hydrological features of the landscape (Von Oppen et al., 2022), *right:* detailed maps of the respective transects with plot locations colored by vegetation unit.

A.4 Study Period

The exact start and end timing of summer periods 2023 and 2024 are shown in Tab. 6. The data set ends on September 11, 2024 at 14:00:00. When comparing the two seasons, I limited the observation period to the overlap of both seasons which is July 24 to September 11.

Table 6: Summer start and end dates for 2023 and 2024. Summer end could not be determined for 2024, since not all soils exhibited frozen conditions for 10 subsequent days within the observation period.

Year	Summer Start	Summer End
2023	2023-07-24 10:45:00	2023-09-20 05:30:00
2024	2024-07-10 13:00:00	-

A.5 Spatial Autocorrelation

Data is spatially autocorrelated, if the proximity of observation points is an indicator for their (dis-)similarity. I calculate the spatial autocorrelation with Moran's I for increasing neighborhood sizes in R using the *spdep* package (Bivand and Piras, 2023). Moran's I measures spatial autocorrelation by examining whether nearby locations have similar or different values compared to the overall mean. Positive values of Moran's I indicate that similar values tend to cluster near each other, while negative values suggest that dissimilar values are more likely to be close together. I defined the neighborhood by distance and calculated Moran's I for each neighborhood size from 0 to 1400 m, increasing the value by 20 m each time. This approach provides a scale-sensitive perspective on spatial autocorrelation in soil temperature data.

The correlogram seen in Fig. 26 reveals highest significant positive spatial autocorrelation ($I >= 0.2$) on the scale of vegetation units (neighborhood size / distance = 20 - 40 m). Considering the length of the transects is 250 m and 285 m respectively, the data is positively and significantly correlated to itself within neighborhoods on the sub-transect scale, but the effect fades when neighborhood size approaches transect size and completely vanishes when each transect is considered its own neighborhood. Only when neighborhood size increases so much that it spans over both transects, I takes on (non-significant) negative values, possibly reflecting the diversity of summer soil temperature means between

both transects. The analysis is limited by the distance between closest neighbors which is ca. 5 m.

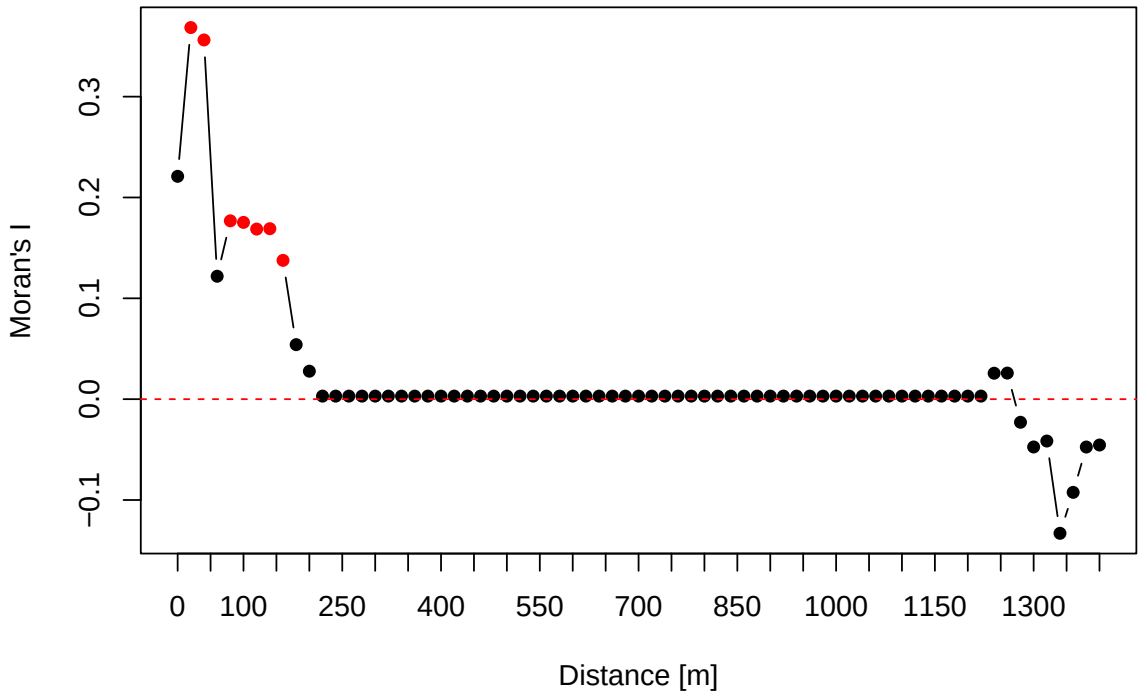

Figure 26: Moran's I as measurement for spatial autocorrelation within mean summer soil temperatures for an increasing neighborhood size (distance). Significant values ($p<0.05$) are colored in red, non-significant in black.

A.6 Extended Results

A.6.1 Long Term Climate Observations

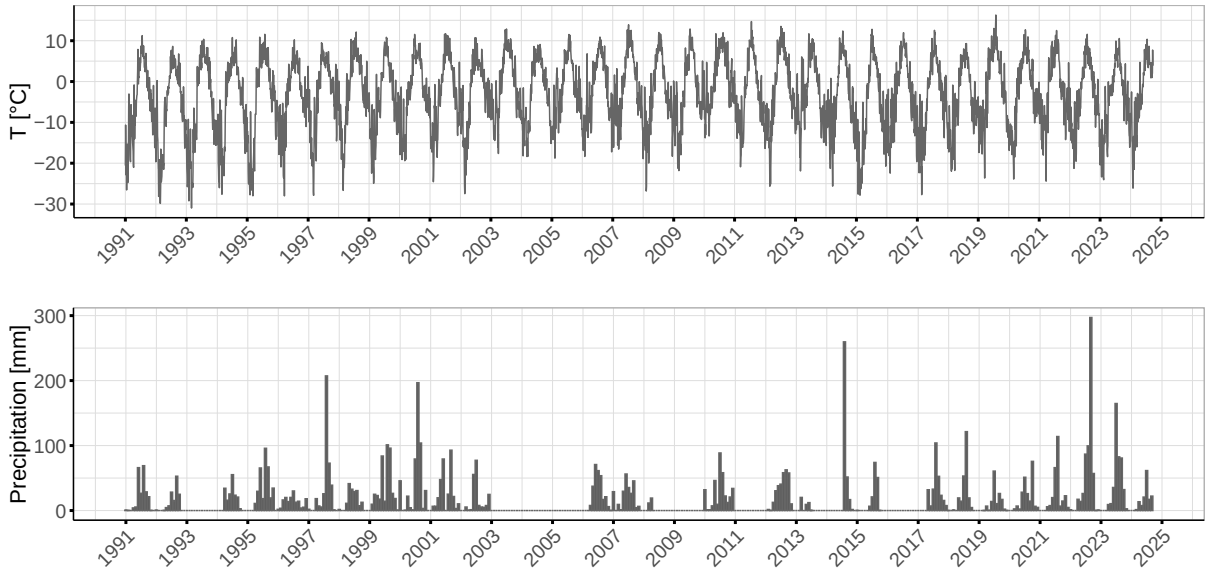

Figure 27: Air temperature and precipitation measured in Blæsedalen in the South of Qeqertarsuaq (Disko Island), Western Greenland, by weather stations AWS1 (1991-2013) and AWS3 (2013-2024). Top: Temperature measurements aggregated to 3-day means. Bottom: Cumulative monthly precipitation.

A.6.2 Spatial and Temporal Variation of Soil Temperature and Moisture

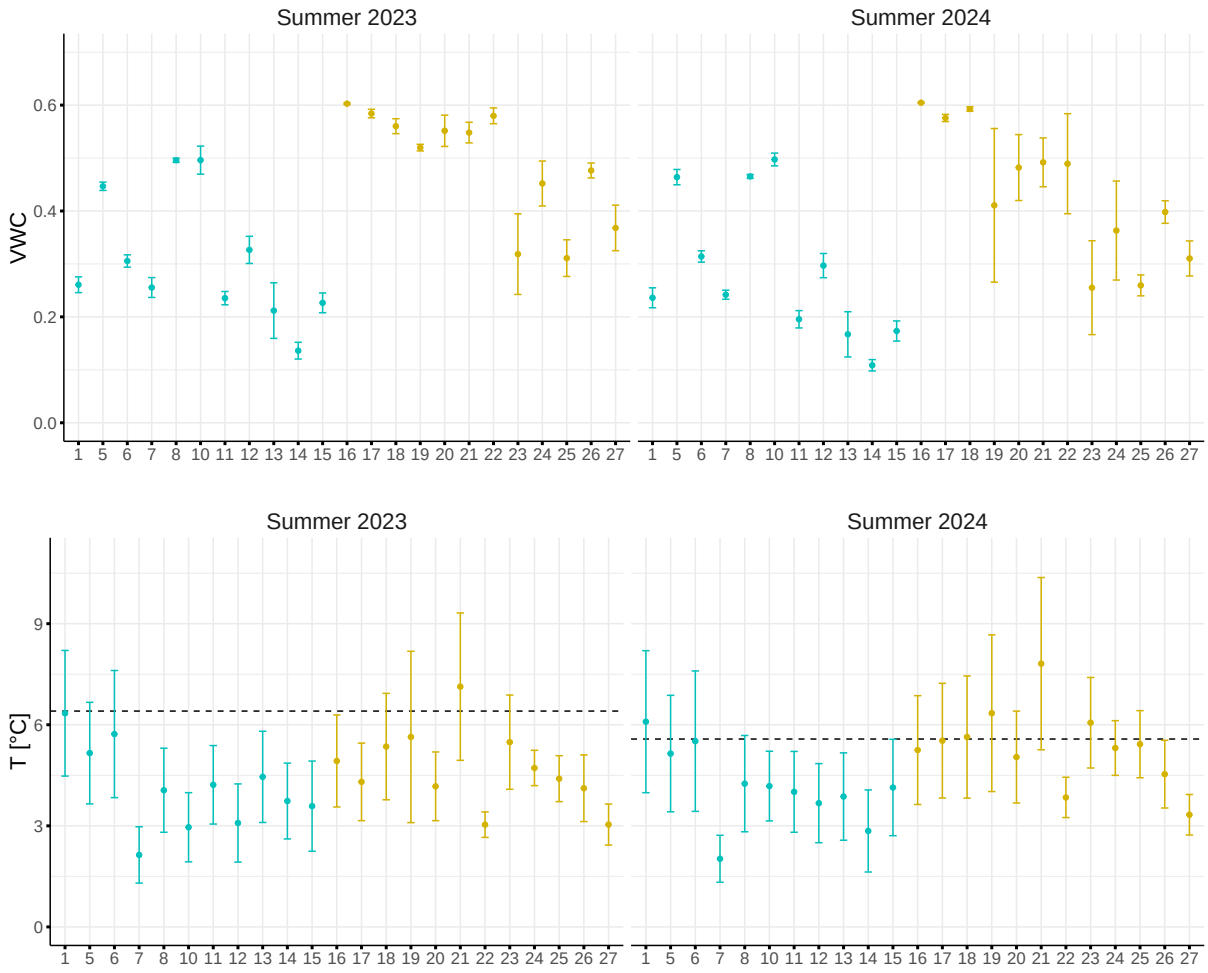

Figure 28: *Above:* Mean soil temperatures with standard deviation at 6 cm depth measured by temperature-moisture sensors during overlapping summer season 2023 and 2024 (for definition of summer see Section A.4). *Below:* Soil moisture given as mean volumetric water content (VWC) of the upper 15 cm of the ground measured by temperature-moisture sensors during summer seasons 2023 and 2024. *Yellow:* Transect 1, *Blue:* Transect 3. Dashed line shows mean air temperature during summer season 2023.

A.6.3 Variable Distributions

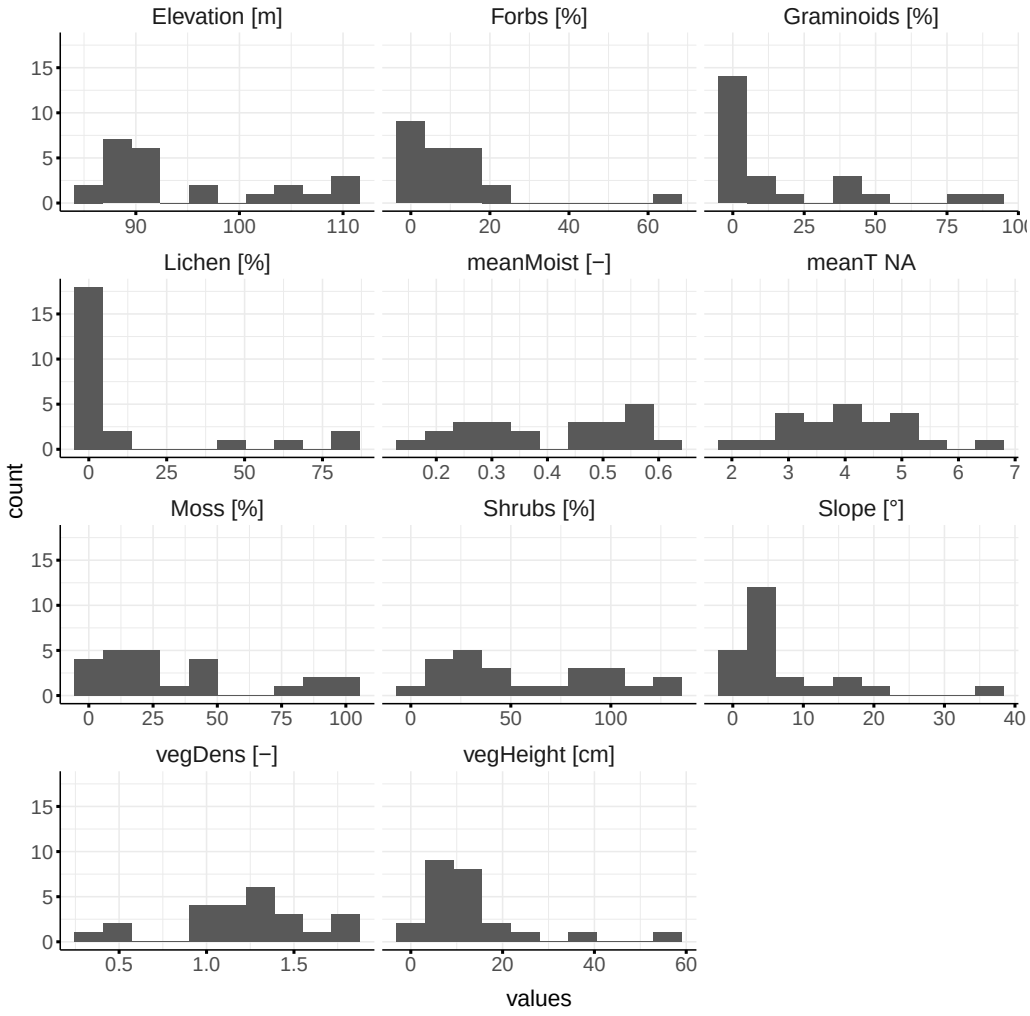

Figure 29: Histogram of all continuous variables used as predictors for linear regression models.

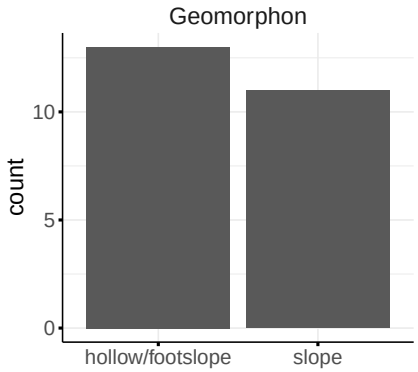

Figure 30: Histogram of the factor variable geomorphon. Of all the geomorphon type classes, only were represented by the plot locations: hollow/footslope and slope.

A.6.4 Linear Model Diagnostics for Moisture

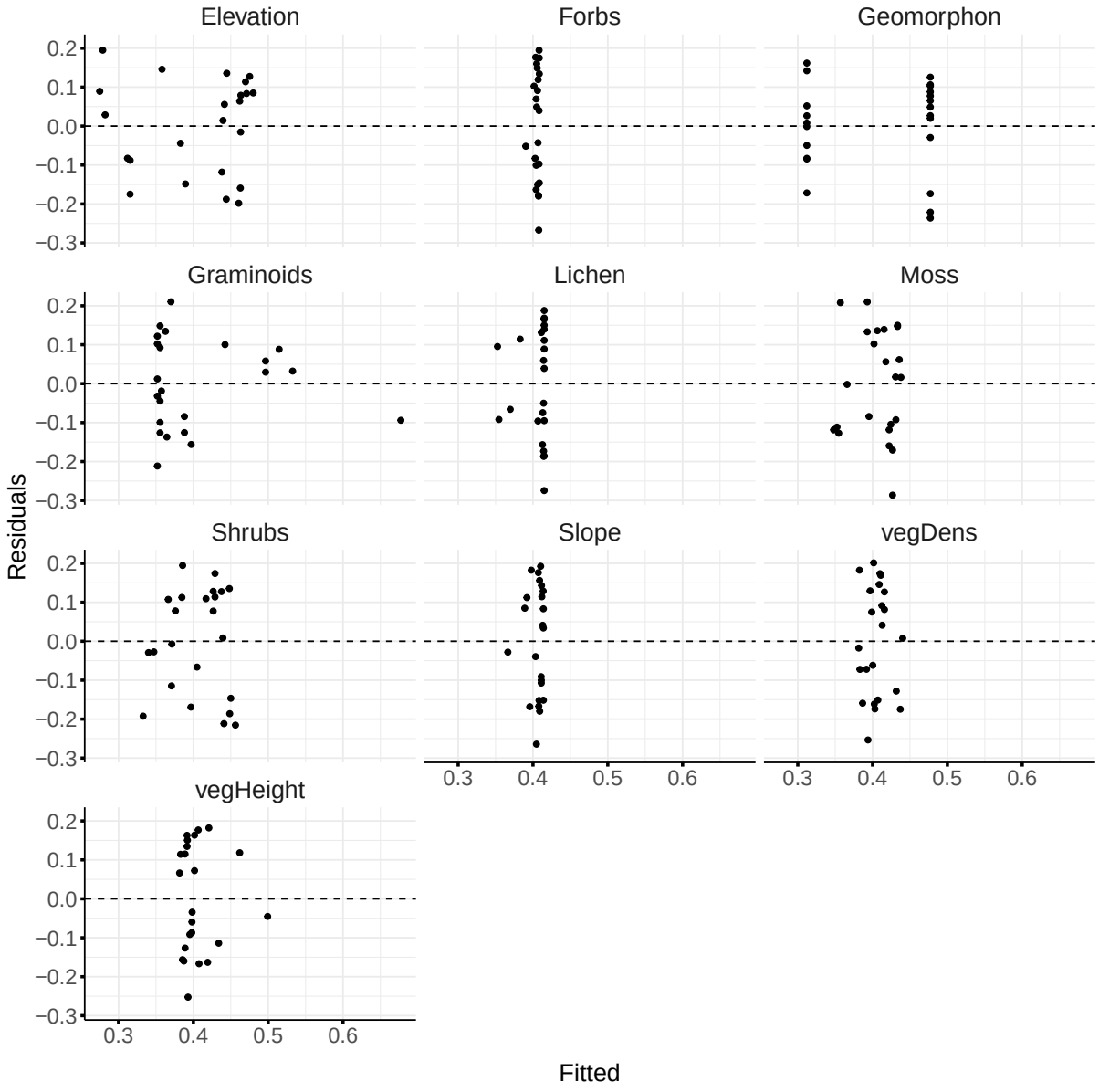

Figure 31: Residual plot showing the relationship between the residuals and predicted values (fitted) of soil moisture. The plot assesses model fit, with residuals distributed randomly around zero indicating no systematic bias.

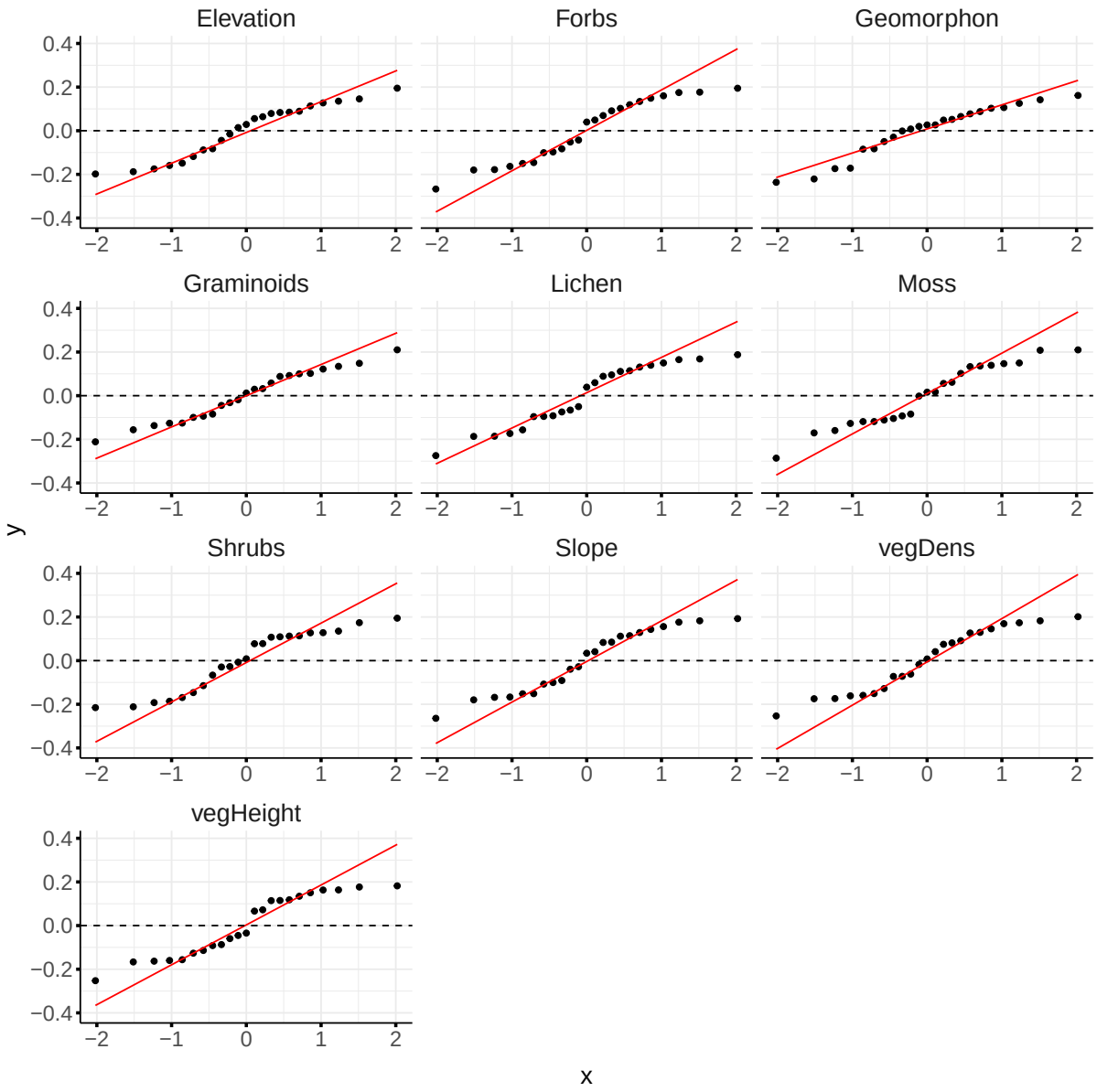

Figure 32: Quantile-Quantile (Q-Q) plot comparing the distribution of residuals (y) to the theoretical normal distribution for all linear regression models predicting soil moisture. Points closely following the red identity reference line indicate that the residuals conform to normality, while deviations suggest departures from the assumption of normality.

A.6.5 Linear Model Diagnostics for Temperature

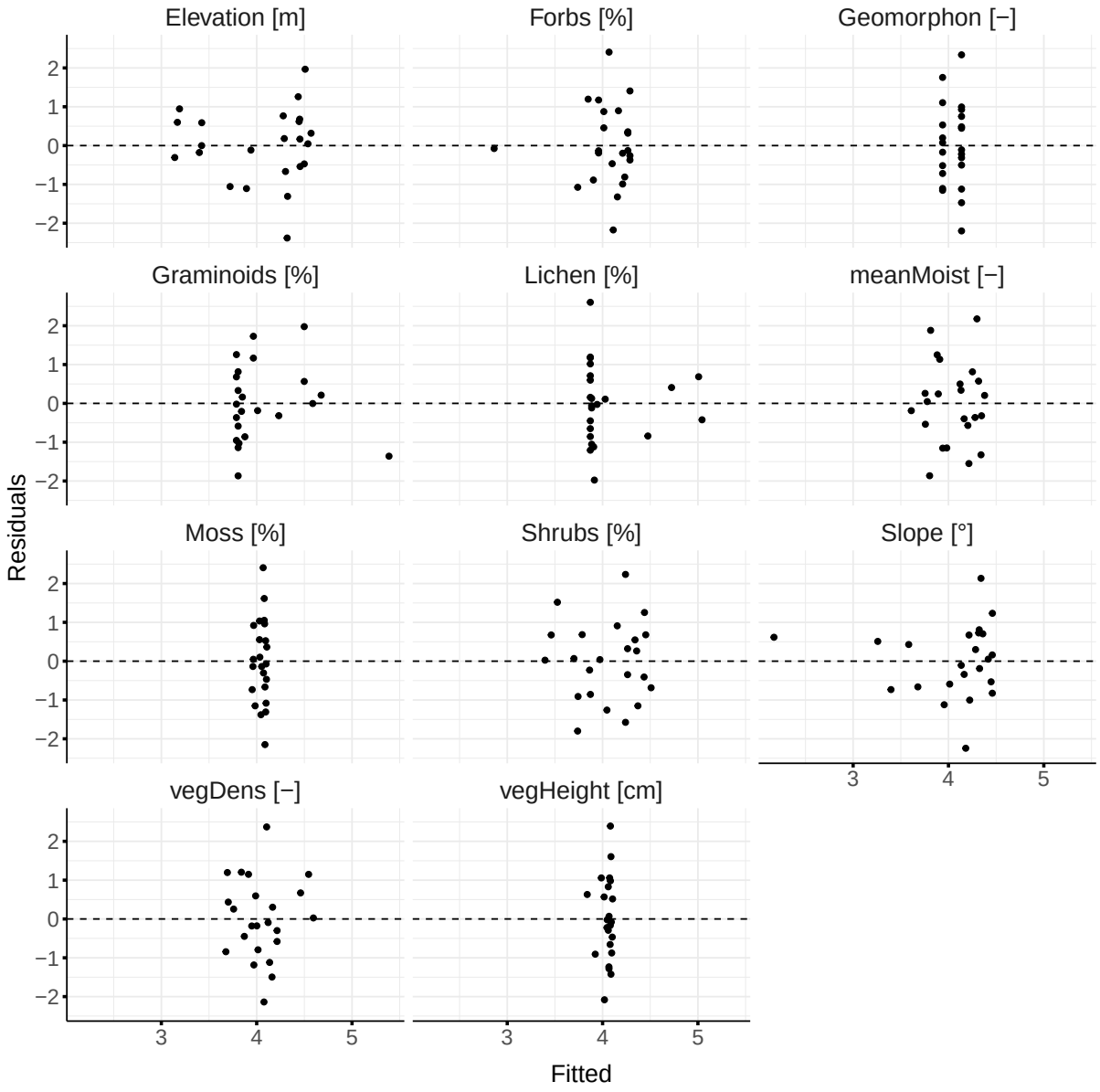

Figure 33: Residual plot showing the relationship between the residuals and predicted values (fitted) of soil temperature. The plot assesses model fit, with residuals distributed randomly around zero indicating no systematic bias.

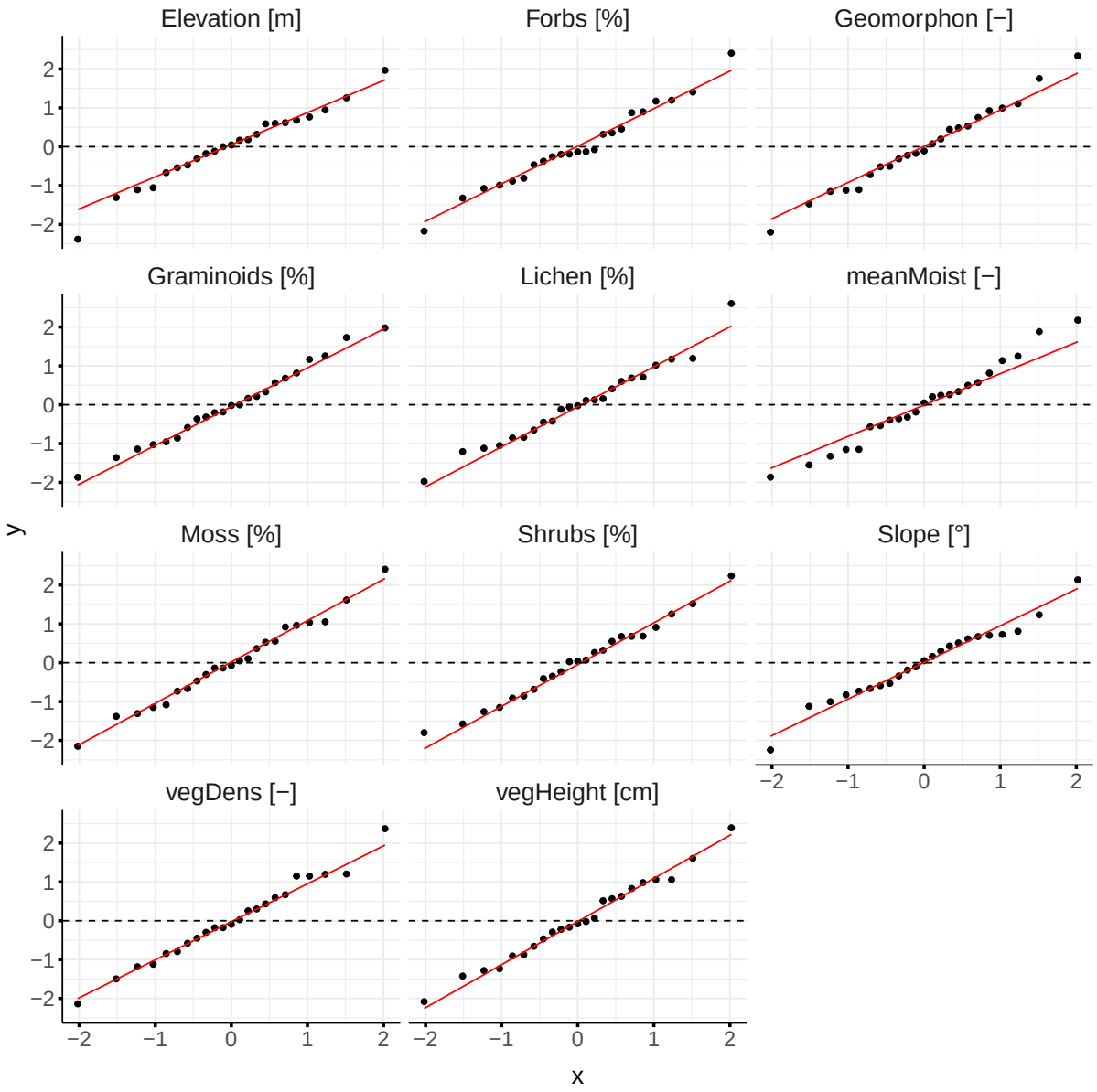

Figure 34: Quantile-Quantile (Q-Q) plot comparing the distribution of residuals (y) to the theoretical normal distribution for all linear regression models predicting soil temperature. Points closely following the red identity reference line indicate that the residuals conform to normality, while deviations suggest departures from the assumption of normality.

Erklärung

Ich erkläre, dass ich die vorliegende Arbeit oder Teile davon nicht für andere Prüfungs- und Studienleistungen eingereicht, selbständig und nur unter Verwendung der angegebenen Literatur und Hilfsmittel angefertigt habe. Sämtliche fremde Quellen inklusive Internetquellen, Grafiken, Tabellen und Bilder, die ich unverändert oder abgewandelt wiedergegeben habe, habe ich als solche kenntlich gemacht. Mir ist bekannt, dass Verstöße gegen diese Grundsätze als Täuschungsversuch bzw. Täuschung geahndet werden.

In Teilen der Arbeit habe ich ChatGPT verwendet, um die Formulierungen meiner eigenen Texte zu verbessern und die grammatikalische Korrektheit zu prüfen.

.....